



Trans. Nonferrous Met. Soc. China 24(2014) 3585-3610

Transactions of Nonferrous Metals Society of China

www.tnmsc.cn

Alloy gene Gibbs energy partition function and equilibrium holographic network phase diagrams of AuCu₃-type sublattice system

You-qing XIE^{1,2,3}, Xiao-bo LI⁴, Xin-bi LIU^{1,2,3}, Yao-zhuang NIE⁵, Hong-jian PENG⁶

- 1. School of Materials Science and Engineering, Central South University, Changsha 410083, China;
 - 2. Powder Metallurgy Research Institute, Central South University, Changsha 410083, China;
- 3. State Key Laboratory of Powder Metallurgy, Central South University, Changsha 410083, China;
- 4. College of Materials Science and Engineering, Xiangtan University, Xiangtan 411105, China;
- 5. School of Physical Physics and Electronics, Central South University, Changsha 410083, China;
- 6. School of Chemistry and Chemical Engineering, Central South University, Changsha 410083, China

Received 5 September 2014; accepted 5 November 2014

Abstract: Taking AuCu₃-type sublattice system as an example, three discoveries have been presented: First, the third barrier hindering the progress in metal materials science is that researchers have got used to recognizing experimental phenomena of alloy phase transitions during extremely slow variation in temperature by equilibrium thinking mode and then taking erroneous knowledge of experimental phenomena as selected information for establishing Gibbs energy function and so-called equilibrium phase diagram. Second, the equilibrium holographic network phase diagrams of AuCu₃-type sublattice system may be used to describe systematic correlativity of the composition—temperature-dependent alloy gene arranging structures and complete thermodynamic properties, and to be a standard for studying experimental subequilibrium order-disorder transition. Third, the equilibrium transition of each alloy is a homogeneous single-phase rather than a heterogeneous two-phase, and there exists a single-phase boundary curve without two-phase region of the ordered and disordered phases; the composition and temperature of the top point on the phase-boundary curve are far away from the ones of the critical point of the AuCu₃ compound.

Key words: AuCu₃ compound; AuCu₃-type sublattice system; alloy gene Gibbs energy partition function; equilibrium holographic network phase diagram; systematic metal materials science

1 Introduction

Early in 1937, SLATER [1] pointed out that "Further progress in the theory is likely to come more and more from cooperation between theoretical physicists and metallurgists, and the advance of physical metallurgy in the next few years is likely to be almost as dependent on the electron theory of metals as the advances of the last generation were dependent on thermodynamics and theory of solutions". Since then, the electron theory of alloy phases has been developed along the quantum mechanical band theory—quantum mechanical abinitio calculations (QMAC)—QMAC-thermodynamics [2–8], then the QMAC-community has been formed. The thermodynamics of alloy phases has been developed along the statistic thermodynamics

of alloy phases—calculation of phase diagrams (CALPHAD)-thermodynamics [9-17],CALPHAD-community has been formed. However, most of the design and testing of alloys are currently performed through time-consuming and repetitive experiment. This situation should be attributed to some existing barriers hindering progress in thermodynamics and electron theory of alloys. In order to discover, develop, manufacture, and deploy advanced materials in a more expeditious and economical way, the materials genome initiative (MGI) was proposed, where the "materials genome" was given a rather vague definition [18]. Recently, the materials genome was defined as "a set of information (databases) allowing predication of a material's structure, as well as its response to processing and usage conditions" [19]. We would say that it is not a good way, because the main barriers hindering the

Corresponding author: You-qing XIE; Tel: +86-731-88879287; E-mail: xieyouq8088@163.com

DOI: 10.1016/S1003-6326(14)63505-6

progress in thermodynamics and electron theory of alloys can not be removed by this way: First, they have not found the alloy gene (AG) sequence and AG-Gibbs energy level sequence, then the AG- Gibbs energy partition function cannot be established, and the real Gibbs energy function cannot be derived; Second, they have not found the reason for keeping structure stabilization of alloys against changing temperature and the atom movement mechanism to change structure for suiting variation in temperature; Third, up to now, researchers have got used to recognizing the experimental phenomena observed during very slow variation in temperature to be thermodynamic equilibrium [20-25], lacking an essential definition of the thermodynamic equilibrium order-disorder transition: 1) The middle jumping T_i -temperature is erroneously considered as the terminal T_c -critical temperature of order-disorder equilibrium transition of the alloy, although the experimental jumping σ_i -order degree is 0.8-0.7, and the experimental short range order degree exists at the temperatures considerable above the T_i temperature; 2) The composition-dependent $T_i(x)$ -points are erroneously considered as the phase boundary points of phase diagram of the AuCu₃-type sublattice system; 3) The heterogeneous "subequilibrium statistic regionscale heterogeneity" with the same composition and different order degrees is erroneously considered two heterogeneous "equilibrium two-phase region" consisting of ordered and disordered phases, and it was pointed out that "if the ordering reaction was a heterogeneous one, the equilibrium diagram would show the ordered phase separated from the disordered phase by a two-phase region" [21]; 4) They hold that the stoichiometric Au₃Cu-, AuCu- and AuCu₃-compounds in the Au₃Cu-, AuCu- and AuCu₃-type sublattice systems have the lowest potential energies at 0 K and the highest $T_{\rm c}$ -critical temperatures on their phase boundary curves, respectively. The researchers in the QMAC-and **CALPHAD-communities** took these erroneous understandings of experimental phenomena as the selected information, then adjusted parameters in Gibbs energy functions and established so-called equilibrium phase diagrams to achieve the best representation of the selected information [19] (see Appendix A.1).

In order to quickly and efficiently discover advanced alloys, the systematic metal materials science (SMMS) was established by new thinking modes and methods of system sciences [26]. Recently, taking AuCu-sublattice system as an example, the AG-sequences, which are the central characteristic atom $A_i^{\rm Au}$ - and $A_i^{\rm Cu}$ - sequences in the basic coordination cluster sequences of the Au–Cu system, were presented, the AG-holographic information database of the

fcc-based lattice Au-Cu system, the AG-Gibbs energy partition function and alloy gene arranging (AGA)-Gibbs energy function of the AuCu-type sublattice system were established, according to AG-Gibbs energy level sequences in the AG-holographic information database, and its equilibrium holographic network phase (EHNP) diagrams were obtained, according to the definition of equilibrium order-disorder transition [27]. Taking experimental path on disordering AuCuI $(A_8^{\text{Au}}A_4^{\text{Cu}})$ composed of the A_8^{Au} and A_4^{Cu} stem alloy genes as an example, three discoveries and a method were presented: 1) The ability of AuCuI ($A_8^{Au}A_4^{Cu}$) to keep structure stabilization against changing temperature is attributed to that the A_8^{Au} and A_4^{Cu} potential well depths greatly surpass their vibration energies, which leads to the subequilibrium of experimental path; 2) A new atom movement mechanism of AuCuI ($A_8^{Au}A_4^{Cu}$) to change structure for suiting variation in temperature is the resonance activating- synchro alternating (RA-SA) mechanism of alloy genes, which leads to heterogeneous and successive subequilibrium transitions; 3) There exists jumping order degree (see Appendix A.2), which leads to the existence of jumping T_i -temperature and an unexpected so-called "retro-effect" about jumping temperature retrograde shift to lower temperatures upon the increasing heating rate. A set of subequilibrium holographic network path charts was obtained by the experimental mixed enthalpy path method [28].

In the present work, taking AuCu₃-type sublattice system as an example, the steps for establishing equilibrium holographic network phase diagrams ((EHNP)-diagrams) and the main characteristics of these EHNP-diagrams have been presented, which are unexpected by today's researchers, and SGTE-database and AG-database, the critical temperature, and the subequilibrium statistic region-scale heterogeneity with the same composition and different order degrees, and equilibrium two-phase region with different composition ordered and disordered phases have been discussed.

2 AG-Gibbs energy partition function

Based on the AG-Gibbs energy sequences and alloy gene arranging (AGA)-Gibbs energy level model, the AG-Gibbs energy partition function of the fcc-based lattice Au–Cu system was established, which is used to describe the systematic correlativity of the AG-Gibbs energy levels ($G_i^{\mathrm{Au}}(T)$, $G_i^{\mathrm{Cu}}(T)$), AG-probabilities ($x_i^{\mathrm{Au}}(x,T,\sigma)$, $x_i^{\mathrm{Cu}}(x,T,\sigma)$) occupied at the AG-Gibbs energy levels and degeneracy factor of the AG-probabilities ($g(x_i^{\mathrm{Au}}(x,T,\sigma),x_i^{\mathrm{Cu}}(x,T,\sigma))$) as functions of the composition (x), temperature (x) and order degree (x):

$$\Omega(x,T,\sigma) = g(x_i^{\text{Au}}(x,T,\sigma), x_i^{\text{Cu}}(x,T,\sigma)) \times \exp[-G^*(x,T,\sigma)/(k_{\text{B}}T)]$$
(1)

where $k_{\rm B}$ is Boltzmann's constant, and $G^*(x,T,\sigma)$ is the characteristic Gibbs energy function of the alloy phase, which may be obtained by the transmission law of the AG-Gibbs energies:

$$G^{*}(x,T,\sigma) = \sum_{i=0}^{12} (x_i^{\text{Au}}(x,T,\sigma) \times G_i^{\text{Au}}(T) + x_i^{\text{Cu}}(x,T,\sigma) \times G_i^{\text{Cu}}(T))$$
(2)

The AGA-total Gibbs energy function of the alloy phase may be derived from the $\Omega(x,T,\sigma)$ -function:

$$G(x,T,\sigma) = -k_{\rm B}T \times \ln(\Omega(x,T,\sigma)) =$$

$$G^*(x,T,\sigma) - TS^{c}(x,T,\sigma)$$
(3)

The total configurational entropy $S^{c}(x,T,\sigma)$ function is obtained from the degeneracy *g*-factor:

$$S^{c}(x,T,\sigma) = k_{B} \ln \{g[x_{i}^{Au}(x,T,\sigma), x_{i}^{Cu}(x,T,\sigma)]\}$$
 (4)

It should be pointed out that these functions may be suitable for Au_3Cu -, AuCu- and $AuCu_3$ -type sublattice systems (σ >0), as well as disordered alloy phase (σ =0) and other type subequilibrium ordered phases, such as the statistic periodic antiphase (SPAP) AuCuII [28,29]. However, their ordering definitions are different, of which the details can be seen in Refs. [27,30].

3 EHNP-diagrams of AuCu₃-type sublattice system

3.1 Essential definition of equilibrium order-disorder

An equilibrium order-disorder transition for a given composition alloy is defined as that "the AG-Gibbs energy levels $(G_i^{Au}(T), G_i^{Cu}(T))$ and AG-probabilities $(x_i^{\text{Au}}(x,T,\sigma),x_i^{\text{Cu}}(x,T,\sigma))$ occupied at the $G_i^{\text{Au}}(T)$ and $G_i^{\text{Cu}}(T)$ -energy levels can respond immediately and change synchronously with each small variation in temperature and proceed along the minimal Gibbs energy path, supposing that there is no obstacle to atom movement". It has following general behaviors: 1) The order-disorder transition upon heating and disorderorder transition upon cooling proceed along the same minimal mixed Gibbs energy $\Delta G_{\min}^{m} - T$ path, namely, there exists no so-called hysteresis phenomenon between both transitions; 2) The $\Delta G_{\min}^{m} - T$ path is continuous and homogenous, and has no jumping phenomenon, namely, single-phase homogeneous transition path; 3) The $T_{\rm c}$ -critical temperature is determined by the crosspoint of $\Delta G_{\rm min}^{\rm m} - T$ and $\Delta G_{\rm dis.}^{\rm m}(x,\sigma=0) - T$ curves, and independent of experimental conditions.

3.2 Steps for establishing EHNP-diagrams

The man's knowledge of relationships of structures, properties and temperature for alloys has been changed from single causality to systematic correlativity, due to the discovery of alloy gene $A_i^{\rm Au}$ - and $A_i^{\rm Cu}$ - sequences and establishment of their AG-information database, as well as AGA-Gibbs energy function derived from the AG-Gibbs energy partition function. The systematic correlativity of the AuCu₃-type sublattice system may be described by a set of EHNP diagrams, which are obtained by following steps:

- 1) According to the $G_i^{Au}(T)$ and $G_i^{Cu}(T)$ level sequences, mixed Gibbs energy $\Delta G^{\rm m}(x,T,\sigma)$ -function and essential definition of equilibrium order-disorder transition, the systematic correlativity of the $\Delta G_{\rm e}^{\rm m}-T$, $\sigma_{\rm e}-T$, $S_{\rm e}^{\rm c}-T$, $x_{i,{\rm e}}^{\rm Au}-T$ and $x_{i,{\rm e}}^{\rm Cu}-T$ paths on equilibrium order-disorder transition as function of temperature for the stoichiometric AuCu₃-alloy are calculated by the minimal mixed Gibbs energy $\Delta G_{\min}^{m} - T$ path method, which includes the iso-order degree Gibbs energy $\Delta G_{\sigma}^{\rm m} - T$ path method (Fig. 1(a)) and the isothermal Gibbs energy $\Delta G_T^{\rm m} - \sigma$ path method (Fig. 1(b)), using calculated steps $\Delta T=1$ K and $\Delta \sigma = 0.0001$. According to the $x_{i,e}^{Au} - T$ and $x_{i,e}^{Cu} - T$ paths, the EHNP charts of the stoichiometric AuCu₃-alloy are calculated by Eqs. (5)–(8) and shown in Appendix B.
- 2) By analogy with the first step, the systematic correlativity data of the $\Delta G_{\rm e}^{\rm m}(x,T)$, $\sigma_{\rm e}(x,T)$, $S^{\rm c}(x,T)$, $x_{i,\rm e}^{\rm Au}(x,T)$ and $x_{i,\rm e}^{\rm Cu}(x,T)$ paths on equilibrium order—disorder transition as function of composition and temperature for alloys of the AuCu₃-type sublattice system are calculated, using calculated steps Δx =0.5% (mole fraction), ΔT =1 K, $\Delta \sigma$ =0.0001.
- 3) According to the systematic correlativity data of the $\Delta G_{\rm e}^{\rm m}(x,T), \quad \sigma_{\rm e}(x,T), \quad S^{\rm c}(x,T), \quad x_{i,\rm e}^{\rm Au}(x,T)$ and $x_{i,\rm e}^{\rm Cu}(x,T), \quad {\rm the} \quad {\rm three-dimensional} \quad \Delta G_{\rm e}^{\rm m}-x-T, \quad \sigma_{\rm e}-x-T, \quad S_{\rm e}^{\rm c}-x-T, \quad x_{i,\rm e}^{\rm Au}-x-T \quad {\rm and} \quad x_{i,\rm e}^{\rm Cu}-x-T$ EHNP diagrams, as well as their two-dimensional q_x-T , T_q-x and q_T-x phase diagrams and configuration entropy EHNP diagrams are constructed and shown in Figs. 2–5.
- 4) According to the first order thermodynamic properties in the AG-database and $x_{i,e}^{Au} x T$ and $x_{i,e}^{Au} x T$ EHNP diagrams, the EHNP diagrams of the first order thermodynamic properties of the AuCu₃-type sublattice system are calculated by their transmission

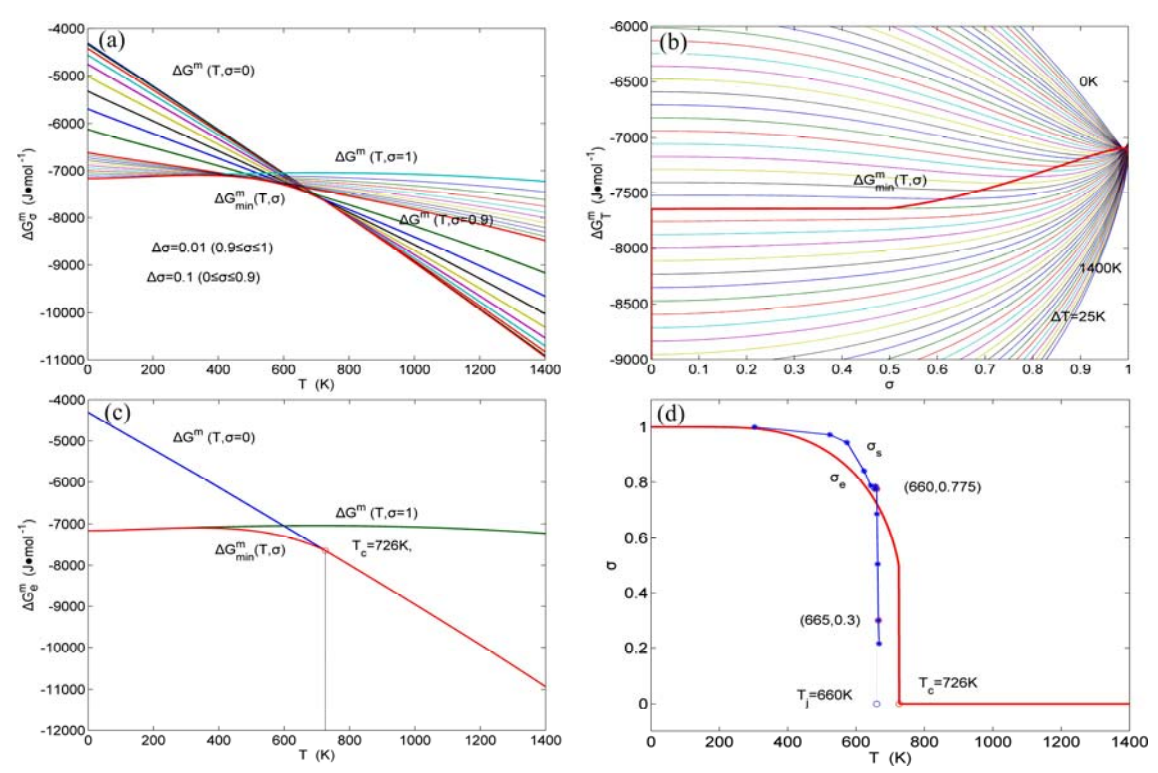


Fig. 1 Minimal mixed Gibbs energy $\Delta G_{\min}^{m} - T$ path on equilibrium order-disorder transition of stoichiometric AuCu₃ alloy: (a) Iso-order degree Gibbs energy $\Delta G_{\sigma}^{m} - T$ path method; (b) Isothermal Gibbs energy $\Delta G_{T}^{m} - \sigma$ path method; (c) $\Delta G_{e}^{m} (\Delta G_{\min}^{m}) - T$ path on equilibrium order-disorder transition of stoichiometric AuCu₃ alloy; (d) $\sigma - T$ path on equilibrium order-disorder transition of stoichiometric AuCu₃ alloy with experimental subequilibrium data [24]

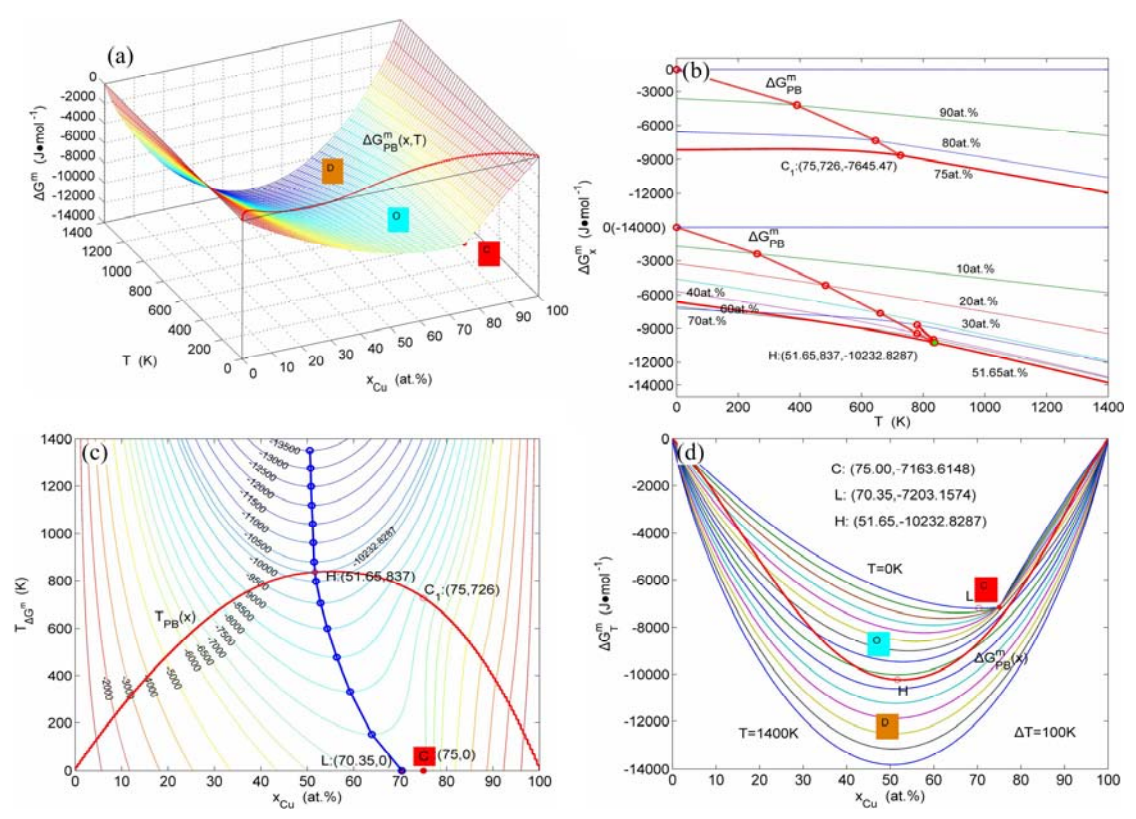


Fig. 2 Mixed Gibbs energy EHNP diagrams of AuCu₃-type sublattice system: (a) Three-dimensional $\Delta G^m - x - T$ diagram with phase boundary curve $\Delta G^{\rm m}_{\rm PB}(x,T)$; (b) Two-dimensional isocompositional $\Delta G^{\rm m}_x - T$ path diagram with phase boundary curve $\Delta G^{\rm m}_{\rm PB}(T)$; (c) Two-dimensional iso-mixed Gibbs energy $T_{\Delta G^{\rm m}} - x$ diagram with phase boundary curve $T_{\rm PB}(x)$; (d) Two-dimensional isothermal $\Delta G^{\rm m}_T - x$ diagram with phase boundary curve $\Delta G^{\rm m}_{\rm PB}(x)$

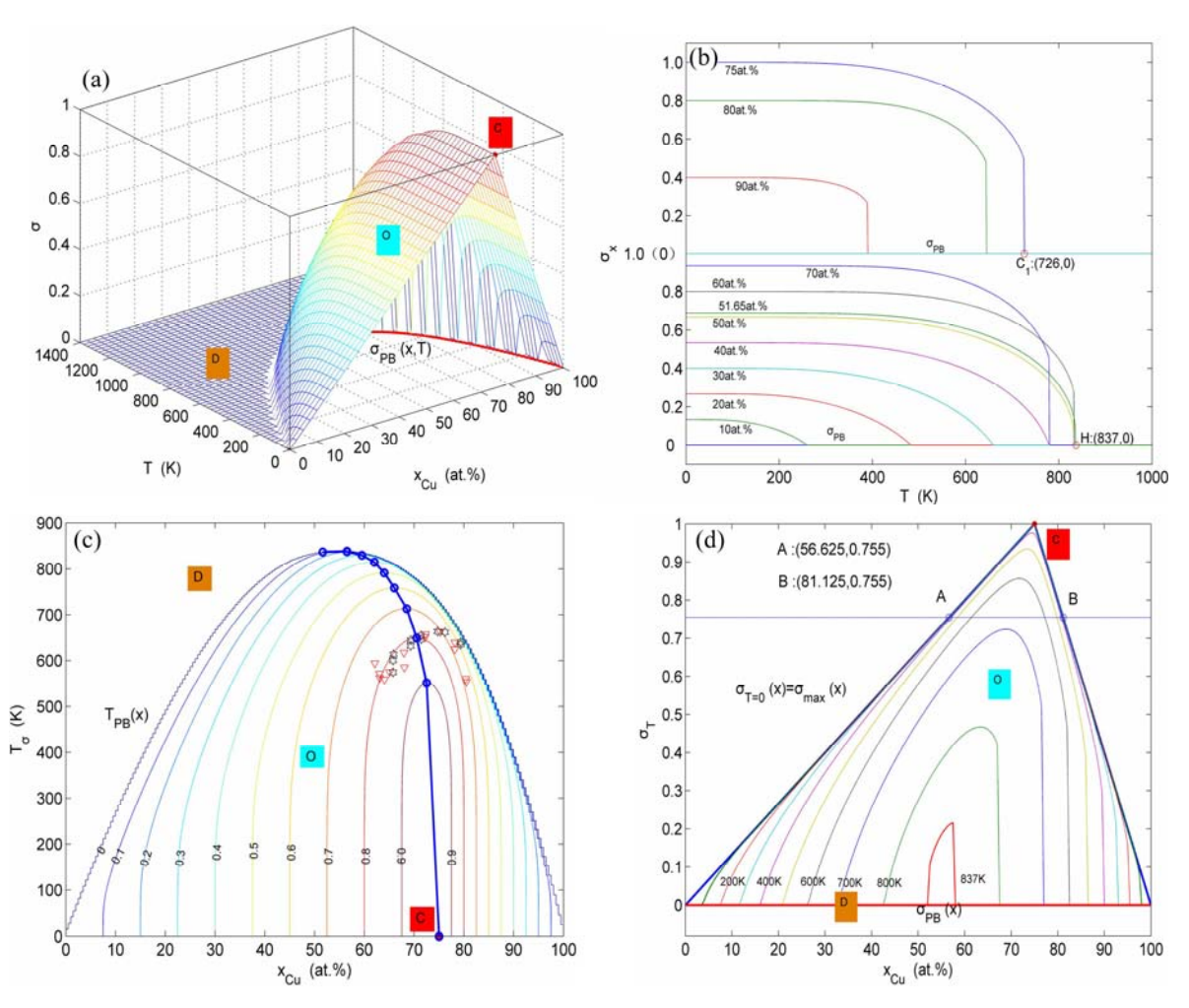


Fig. 3 Order degree EHNP diagrams of AuCu₃-type sublattice system: (a) Three-dimensional σ -x-T diagrams with phase boundary curve $\sigma_{PB}(x, T)$; (b) Two-dimensional isocompositional σ_x -T path diagrams with phase boundary curve $\sigma_{PB}(T)$; (c) Two-dimensional iso-order degree T_σ -x diagrams with phase boundary curve $T_{PB}(x)$; (d) Two-dimension isothermal σ_T -x diagram with phase boundary curve $\sigma_{PB}(x)$

laws, which may be also called as the additive law of extensive *q*-properties of characteristic crystals [31]:

$$\begin{cases} q(x,T,\sigma) = \sum_{i=0}^{I} x_{i}^{\text{Au}}(x,T,\sigma)q_{i}^{\text{Au}}(T) + \\ \sum_{i=0}^{I} x_{i}^{\text{Cu}}(x,T,\sigma)q_{i}^{\text{Cu}}(T) \\ q_{\text{Au}}(x,T,\sigma) = \sum_{i=0}^{I} x_{i}^{\text{Au}}(x,T,\sigma)q_{i}^{\text{Au}}(T)/x_{\text{Au}} \\ q_{\text{Cu}}(x,T,\sigma) = \sum_{i=0}^{I} x_{i}^{\text{Cu}}(x,T,\sigma)q_{i}^{\text{Cu}}(T)/x_{\text{Cu}} \end{cases}$$
(5)

where q denotes characteristic Gibbs energy (G^*) , enthalpy (H), potential energy (E), volume (v), generalized vibration free energy (X^v) , generalized vibration energy (U^v) or generalized vibration entropy (S^v) .

5) The EHNP diagrams of the second order thermodynamic properties (mixed heat capacity and

mixed volume expansion coefficient) are calculated by following equations [27]:

$$\Delta c_{p}^{\mathrm{m}}(x,T,\sigma) = \Delta c_{p}^{\mathrm{m.v}}(x,T,\sigma) + \Delta c_{p}^{\mathrm{m.s}}(x,T,\sigma)$$

$$\Delta c_{p}^{\mathrm{m.v}}(x,T,\sigma) = \sum_{i=0}^{I} x_{i}^{\mathrm{Au}}(x,T,\sigma) (c_{p,i}^{\mathrm{Au.v}}(T) - c_{p,0}^{\mathrm{Au.v}}(T)) +$$

$$\sum_{i=0}^{I} x_{i}^{\mathrm{Cu}}(x,T,\sigma) (c_{p,i}^{\mathrm{Cu.v}}(T) - c_{p,12}^{\mathrm{Cu.v}}(T))$$

$$\Delta c_{p}^{\mathrm{m.s}}(x,T,\sigma) = \sum_{i=0}^{I} \frac{\partial x_{i}^{\mathrm{Au}}(x,T,\sigma)}{\partial \sigma} \cdot$$

$$\frac{\mathrm{d}\sigma}{\mathrm{d}T} (H_{i}^{\mathrm{Au}}(T) - H_{0}^{\mathrm{Au}}(T)) +$$

$$\sum_{i=0}^{I} \frac{\partial x_{i}^{\mathrm{Cu}}(x,T,\sigma)}{\partial \sigma} \cdot$$

$$\frac{\mathrm{d}\sigma}{\mathrm{d}T} (H_{i}^{\mathrm{Cu}}(T) - H_{12}^{\mathrm{Cu}}(T))$$

(6)

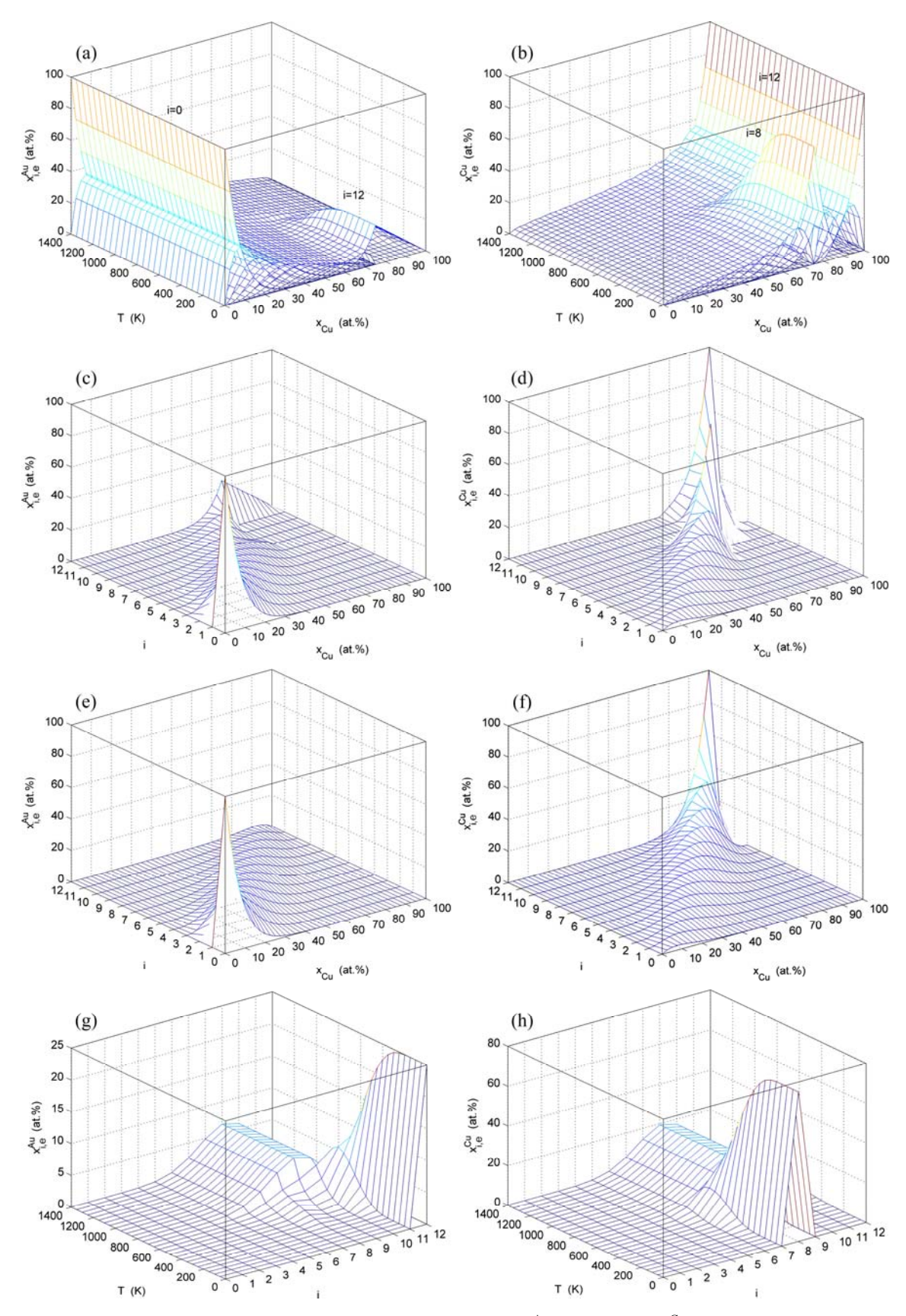


Fig. 4 AG-concentration EHNP diagrams: (a, b) Three-dimensional $x_{i,e}^{Au} - x - T$ and $x_{i,e}^{Cu} - x - T$ diagrams; (c, d) Three-dimensional $x_{i,e}^{Au} - x - i$ and $x_{i,e}^{Cu} - x - i$ diagrams of ordered $Au_{(1-x)}Cu_x$ alloys with maximum order degree σ_{max} at 0 K; (e, f) Three-dimensional $x_{i,e}^{Au} - x - i$ and $x_{i,e}^{Cu} - x - i$ diagrams of perfectly disordered $Au_{(1-x)}Cu_x$ alloys; (g, h) Three-dimensional $x_{i,e}^{Au} - T - i$ and $x_{i,e}^{Cu} - T - i$ path charts on disordering or ordering stoichiometric $AuCu_3$ alloy

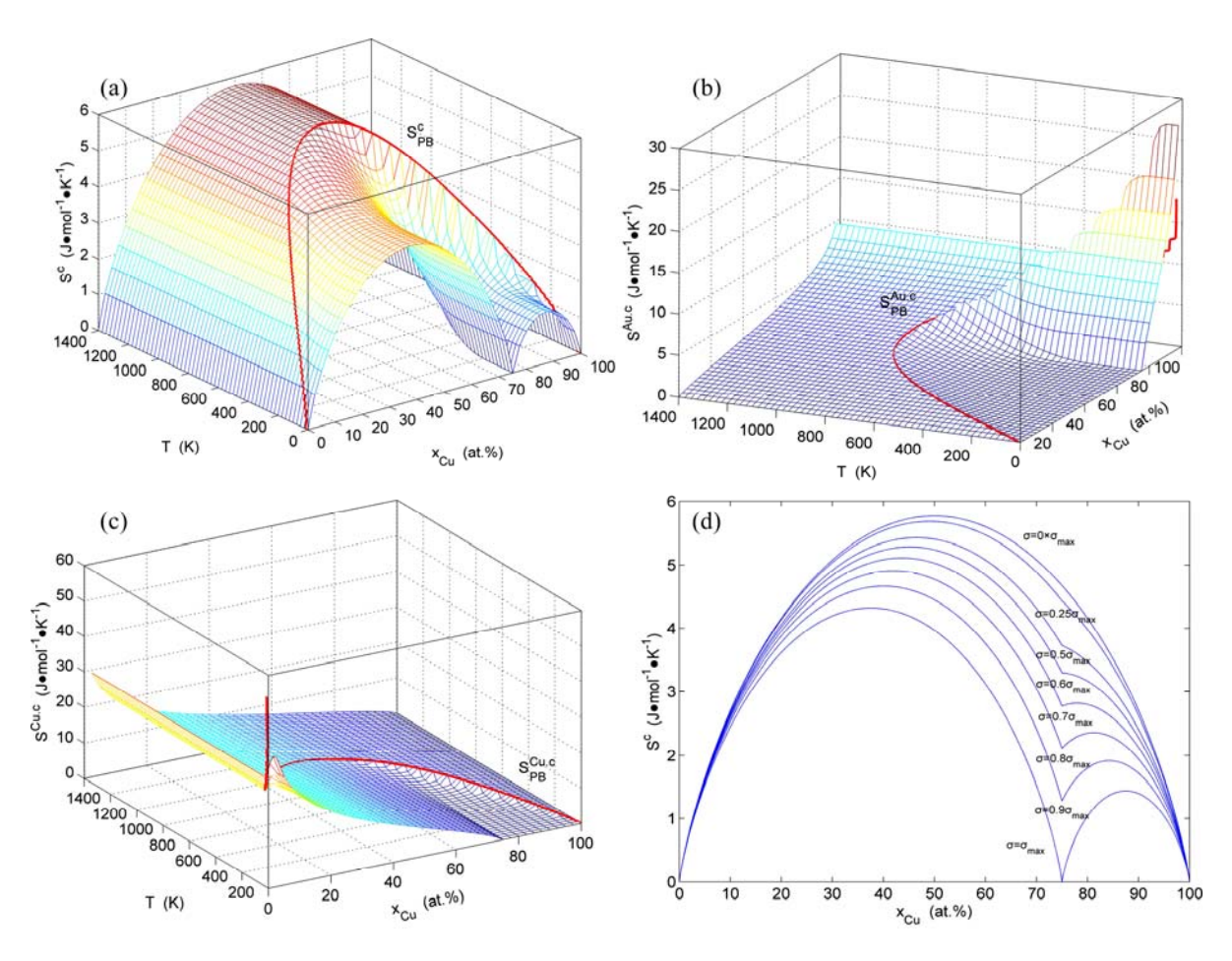


Fig. 5 Configuration entropy EHNP diagrams of AuCu₃-type sublattice system: (a) Three-dimensional $S^c - x - T$ phase diagram with phase boundary curve $S_{PB}^c(x,T)$; (b) Three-dimensional $S^{Au.c} - x - T$ phase diagram with phase boundary curve $S_{PB}^{Au.c}(x,T)$ of Au-component; (c) Three-dimensional $S^{Cu.c} - x - T$ diagram with phase boundary curve $S_{PB}^{.Cu.c}(x,T)$ of Cu-component; (d) $S^c(x,\sigma)$ curves at different σ values as function of $\sigma_{max}(x)$

$$\Delta \beta^{\mathrm{m}}(x,T,\sigma) = \Delta \beta^{\mathrm{m},\mathrm{v}}(x,T,\sigma) + \Delta \beta^{\mathrm{m},\mathrm{s}}(x,T,\sigma)$$

$$\Delta \beta^{\mathrm{m},\mathrm{v}}(x,T,\sigma) = \sum_{i=0}^{I} x_{i}^{\mathrm{A}\mathrm{u}}(x,T,\sigma) [\beta_{i}^{\mathrm{A}\mathrm{u},\mathrm{v}}(T) - \beta_{0}^{\mathrm{A}\mathrm{u},\mathrm{v}}(T)] + \sum_{i=0}^{I} x_{i}^{\mathrm{C}\mathrm{u}}(x,T,\sigma) [\beta_{i}^{\mathrm{C}\mathrm{u},\mathrm{v}}(T) - \beta_{12}^{\mathrm{C}\mathrm{u},\mathrm{v}}(T)]$$

$$\Delta \beta^{\mathrm{m},\mathrm{s}}(x,T) = \sum_{i=0}^{I} \left(\frac{1}{v_{i}^{\mathrm{A}\mathrm{u}}(T)}\right) \frac{\partial x_{i}^{\mathrm{A}\mathrm{u}}(x,T,\sigma)}{\partial \sigma} \cdot \frac{\partial \sigma}{\partial \sigma}$$

$$\frac{\mathrm{d}\sigma}{\mathrm{d}T} [v_{i}^{\mathrm{A}\mathrm{u}}(T) - v_{0}^{\mathrm{A}\mathrm{u}}(T)] + \sum_{i=0}^{I} \left(\frac{1}{v_{i}^{\mathrm{C}\mathrm{u}}(T)}\right) \frac{\partial x_{i}^{\mathrm{C}\mathrm{u}}(x,T,\sigma)}{\partial \sigma} \cdot \frac{\partial \sigma}{\partial \sigma}$$

$$\frac{\mathrm{d}\sigma}{\mathrm{d}T} [v_{i}^{\mathrm{C}\mathrm{u}}(T) - v_{12}^{\mathrm{C}\mathrm{u}}(T)]$$
(7)

6) The EHNP diagrams of the activities of the Auand Cu-components are calculated by following equation [27]:

$$\begin{cases} a_{\text{Au}}(x, T, \sigma) = x_{\text{Au}} \cdot \exp[\Delta G_{\text{Au}}^{*\text{m}}(x, T, \sigma) / (RT)] \\ a_{\text{Cu}}(x, T, \sigma) = x_{\text{Cu}} \cdot \exp[\Delta G_{\text{Cu}}^{*\text{m}}(x, T, \sigma) / (RT)] \\ \Delta G^{*\text{Au}}(x, T, \sigma) = \\ (1/x_{\text{Au}}) \sum_{i=0}^{I=12} x_i^{\text{Au}}(x, T, \sigma) [G_i^{\text{Au}}(T) - G_0^{\text{Au}}(T)] \\ \Delta G^{*\text{Cu}}(x, T, \sigma) = \\ (1/x_{\text{Cu}}) \sum_{i=0}^{I=12} x_i^{\text{Cu}}(x, T, \sigma) [G_i^{\text{Cu}}(T) - G_I^{\text{Cu}}(T)] \end{cases}$$
(8)

- 7) The composition–temperature-dependent $\Delta G_{\rm PB}^{\rm m}-x-T$, $(x_{i,\rm e}^{\rm Au})_{\rm PB}-x-T$ and $(x_{i,\rm e}^{\rm Cu})_{\rm PB}$ –x-T phase boundary (PB) curves are calculated by difference method of Gibbs energies between ordered and disordered phases (see Appendix A.4).
- 8) According to the $(x_{i,e}^{Au})_{PB} x T$ and $(x_{i,e}^{Cu})_{PB} x T$ phase boundary curves, the other $q_{PB} x T$ phase boundary curves are calculated by Eqs. (5)–(8).

3.3 Mixed Gibbs energy EHNP diagrams

The mixed Gibbs energy EHNP diagrams include a three-dimensional $\Delta G^{\rm m}-x-T$ network phase diagram and three two-dimensional $\Delta G_x^{\rm m}-T$, $T_{\Delta G^{\rm m}}-x$ and $\Delta G_T^{\rm m}-x$ path network phase diagrams (Fig. 2). In these diagrams, once one network point $(x,T,\Delta G^{\rm m})$ has been clicked, the information about composition (x), temperature (T) and mixed Gibbs energy $(\Delta G^{\rm m})$ may be readily obtained.

From Fig. 2(a), the following main understandings may be obtained: 1) There are ordered single-phase region with Gibbs energy network points (denoted by the symbol "O") and disordered single-phase region with Gibbs energy network points (denoted by the symbol "D"). 2) The $\Delta G_{PB}^{m}(x,T)$ -phase boundary (PB) curve with Gibbs energy network points is obtained by difference method of Gibbs energies between ordered and disordered phases. By this method, it has been proved that there is a single-phase boundary curve rather than a boundary two-phase region of ordered and disordered phases (see Appendix A.4). 3) The equilibrium state of the stoichiometric AuCu₃ compound, of which the alloy gene arranging (AGA)-molecular formula is the $A_{12}^{Au}(A_{8}^{Cu})_{3}$, exists only at the network C-point ($x_{Cu}=75\%$, T=0 K, $\Delta G^{m}=\Delta E=-7163.61$ J/mol).

From Fig. 2(b), the following main understandings may be obtained: 1) The critical network point of the stoichiometric AuCu₃ alloy, i.e., phase boundary point is located at the network C-point (x_{Cu} =75%, T_{c} =726 K, ΔG =-7645.47 J/mol). 2) The Au_{48.35}Cu_{51.65} alloy has the highest critical temperature in the AuCu₃-type sublattice system, it is located at the network H-point (x_{Cu} =51.65%, T_{c} =837 K, ΔG ^m=-10232.83 J/mol). 3) The equilibrium $\Delta G_{x,\text{e}}^{\text{m}} - T$ path for a given composition (x) alloy is the standard path for determining Gibbs energy hysteresis effect, i.e., superheated and undercooled driving Gibbs energies ($\Delta G_{x,\text{e}}^{\text{m}}(T) - \Delta G_{x,\text{s}}^{\text{m}}(T)$) of experimental $\Delta G_{x,\text{s}}^{\text{m}}(T)$ -path.

From Fig. 2(c), we can know that the lowest temperature points of the iso-mixed Gibbs energy $T_{\Delta G^{\rm m}} - x$ curves move from the network L-point ($x_{\rm Cu}$ =70.35%, T=0 K, $\Delta G^{\rm m}$ = $\Delta E^{\rm m}$ =-7203.16 J/mol) to the network H-point ($x_{\rm Cu}$ =51.65%, $T_{\rm c}$ =837 K, $\Delta G^{\rm m}$ =-101232.83 J/mol), that is unexpected by today's researchers.

From Fig. 2(d), we can know that the $Au_{29.65}Cu_{70.35}$ alloy with the lowest potential energy is located at the network L-point, it slightly deviates from the C-point, that is also unexpected by today's researchers. This diagram will be used to establish EHNP diagrams of the Au–Cu system together with isothermal $\Delta G_T^{\rm m} - x$ diagrams of the AuCu-type and Au₃Cu-type sublattice systems.

3.4 Order degree EHNP diagrams

The order degree EHNP diagrams include a three-dimensional σ -x-T network phase diagram and three two-dimensional σ_x -T, T_σ -x and σ_T -x path network phase diagrams (Fig. 3). In these diagrams, once one network point has been clicked, the information about composition (x), temperature (T) and order degree (σ), as well as the mixed Gibbs energy (ΔG ^m) may be readily obtained, because the order degree EHNP diagrams have been attached to the mixed Gibbs energy EHNP diagrams.

From Fig. 3(a), the following main understandings may be obtained: 1) There are ordered phase region with order degree network points (denoted by the symbol "O", σ >0), disordered phase region (denoted by the symbol "D", σ =0) and $\sigma_{\text{PB}}(x, T)$ -phase boundary (PB) curve (σ =0). 2) The equilibrium state of the $A_{12}^{\text{Au}}(A_8^{\text{Cu}})_3$ compound exists only at the network C-point (x_{Cu} =75%, T=0 K, σ =1).

From Fig. 3(b), we can know that: 1) The equilibrium $\sigma_{x,e}-T$ paths of alloys on the Au-rich side of the $A_{12}^{Au}(A_8^{Cu})_3$ compound have great difference from the ones of alloys on the Cu-rich side of the $A_{12}^{Au}(A_8^{Cu})_3$ compound. 2) The Au_{48.35}Cu_{51.65} alloy in the single AuCu₃-type sublattice system has the highest critical temperature, its network H-point (x_{Cu} =51.65%, T_c =837 K, σ =0) deviates far from the network point (x_{Cu} =75%, T_c =663 K, σ =0) of stoichiometric AuCu₃ alloy. However, their network points are respectively (x_{Cu} =51.65%, σ =0.6887) and (x_{Cu} =75%, σ =1) at 0 K. 3) The equilibrium $\sigma_{x,e}$ – T path for a given composition (x_{Cu}) alloy is the standard path for studying subequilibrium $\sigma_{x,s}$ – T paths. These phenomena can not be expected in the QMAC- and CALPHAD-thermodynamics.

From Fig. 3(c), we have discovered surprising phenomena: 1) All experimental middle jumping T_i —temperatures (denoted by symbols """ [32] and """ [33], which were erroneously considered the so-called T'_{c} -critical temperatures of equilibrium order-disorder transition of alloys, approach to equilibrium iso-order degree $T_{\sigma=0.8} - x$ curve. For the stoichiometric AuCu₃ alloy, the experimental jumping order degree is σ_i =0.775 at the jumping temperature T_i =660 K and the low order degree is σ_L =0.3 at T=665 K (Fig. 1(d)) [24], as well as that the short-range order degree persists to $T_{\rm i}$ -temperature [25]. Therefore, experimental jumping temperature cannot represent the critical temperature of equilibrium order-disorder transition. 2) The highest temperature points of the iso-order degree T_{σ} -x curves move from the network C-point ($x_{\text{Cu}}=75\%$, T=0 K, $\sigma=1$) to the network H-point $(x_{\text{Cu}} = 51.65\%, T_{\text{c}} = 837 \text{ K}, \sigma = 0).$

Figure 3 (d) shows that the network points of alloys

with jumping-phenomena of order-disorder transition should be situated in the range from A-point to B-point, i.e., $0.755 \le \sigma \le 1$ and $56.625\% \le x_{Cu} \le 81.125\%$. These phenomena show that the experimental order–disorder transition belongs to subequilibrium.

3.5 AG-concentration EHNP diagrams

From Fig. 4, the following main understandings may be obtained: 1) The AG-concentration EHNP diagrams, which are used to describe the AG-arranging structures of alloy phases, may be described by two modes: three-dimensional $x_i^{Au} - x - T$ and $x_i^{Cu} - x - T$ network phase diagrams (Figs. 4(a) and (b)) in the AGAcrystallography [34], where the x_i^{Au} and x_i^{Cu} are the probabilities occupied at the lattice points; three-dimensional $x_i^{\rm Au}-x-i$ and $x_i^{\rm Cu}-x-i$ network phase diagrams, (Figs. 4(c) and (d)) in the AGA-Gibbs energy level theory, where the x_i^{Au} and x_i^{Cu} are the probabilities occupied at the $G_i^{Au}(T)$ and $G_i^{Cu}(T)$ energy levels. 2) There exists an emergent phenomenon of some AG-concentrations in the ordered alloy phases, which are defined as that some AG-concentrations in the ordered state are larger than thoes in disorder state, such as x_{12}^{Au} , x_{11}^{Au} , x_{8}^{Cu} and x_{7}^{Cu} (Figs. 4(c), (d), (e) and (f)). 3) The equilibrium $x_{i,\text{e}}^{\text{Au}} - T$ and $x_{i,\text{e}}^{\text{Cu}} - T$ paths for a given composition (x) alloy may be described by $x_i^{\text{Au}} - x - i$ and $x_i^{\text{Cu}} - x - i$ three-dimensional equilibrium path charts (Figs. 4(g) and (h)) or two-dimensional $(x_i^{\text{Au}})_{\sigma} - i$ and $(x_i^{\text{Cu}})_{\sigma} - i$, as well as $(x_i^{\text{Au}}) - \sigma$ and $(x_i^{\text{Cu}}) - \sigma$ equilibrium path charts. The essential on disordering $A_{12}^{\text{Au}}(A_8^{\text{Cu}})_3$ compound is that the A_{12}^{Au} and A_8^{Cu} stem alloy genes are split into A_i^{Au} and A_i^{Cu} sequences in the disordered state. 4) It can be known that each kind of q-EHNP diagram includes not only the 4-type diagrams indicated above, but also other-type diagrams. These AG-concentration equilibrium path charts will provide standard path charts for studying kinetic mechanism of experimental subequilibrium order-disorder transition path.

3.6 Configuration entropy EHNP diagrams

The configuration entropy ($S^c(x,T)$) EHNP diagrams have been established, based on the degeneracy $g(x_i^{\text{Au}}(x,T),x_i^{\text{Cu}}(x,T))$ -function in the AG-Gibbs energy partition $\Omega(x,T)$ -function. From Fig. 5, we have obtained following main understandings: 1) The configuration entropy of each ordered alloy can change continually from the configuration entropy of the maximum order degree σ_{max} state to one of the ideal disordered states. It means that we should take the ideal disordered state as the standard. 2) The structural units used for calculating configuration entropy should be in agreement with the structural units used for calculating corresponding Gibbs

energy levels. These are two rules to establish partition function. However, these rules are often neglected in the currently used thermodynamic models of the QMAC-and CALPHAD-thermodynamics.

3.7 EHNP diagrams of other thermodynamic properties

According to $x_i^{Au} - x - T$ and $x_i^{Cu} - x - T$ EHNP diagrams obtained from $\Delta G^{m} - x - T$ diagram, we have obtained q-x-T EHNP diagrams of other thermodynamic properties of AuCu₃-type sublattice system, which are shown in Appendix C. It should be emphasized that from each three-dimensional q - x - TEHNP diagram, we can obtain isocompositional $q_x - T$, isoproperty $T_q - x$ and isothermal $q_T - x$ path phase diagrams. The diagrams from Section 3.3 through the present section are interconnected to form a big holographic network information database about structures, properties and their variations with composition and temperature of alloys. Therefore, the knowledge of relationships of structures, properties and environments for alloys has been changed from single causality to systematic correlativity. Once one network point in any EHNP diagram above has been clicked, the information about composition, temperature, order degree, AGA-structure and a set of thermodynamic properties of the alloy as well as its equilibrium order-disorder transition EHNP charts may be readily obtained, which are very useful for materials engineers to design advanced alloys.

4 Discussion

4.1 Discussion on SGTE-database and AGholographic information database

The SGTE-database established by Scientific Group Thermodata Europe compile Gibbs energies, i.e., the so-called lattice stability, of 78 pure elements with fcc, hcp and bcc based lattices and liquid state are tabulated, which are widely adopted within the CALPHAD-community. The SGTE-Gibbs energy function is represented as a power series in terms of temperature T in form of $G=a+bT+cT\ln(T)+\sum dT^n$. From this expression, other thermodynamic functions can be evaluated [35]. However, it does not reveal the essence of Gibbs energies of pure elements.

The AG-holographic information database includes the potential energies and volumes of AG-sequences at 0 K temperature obtained by the separated theory of potential energies and volumes of characteristic atoms, the valence electron structures and physical properties of AG-sequences obtained by the valence bond theory of characteristic crystals and the thermodynamic properties of AG-sequences obtained by the thermodynamics of characteristic crystals [27]. The flow charts for establishing AG-holographic information database of the fcc-based lattice Au-Cu system are presented in Appendix D. The AG-holographic information database has following characteristics: 1) In the Au-Cu system with fcc-based lattice, the primary C_0^{Au} - and C_{12}^{Cu} characteristic crystals are respectively the pure Au-metal and pure Cu-metal with fcc-based lattice. The Gibbs energy function of pure metals in the SGTE-database is equivalent to the AG-Gibbs energy function of the primary characteristic crystals. However, the AG-Gibbs energy function is a complex function, i.e., $G_i\left(T,E_i,H_i,X_i,U_i^{v},S_i^{v},c_{p_i}^{v},\theta_i\right)$ obtained from other thermodynamic properties, which reveals the essence of AG-Gibbs energies. 2) The AG-holographic information database of the fcc-based lattice Au-Cu system may be used to establish equilibrium and subequilibrium holographic network phase diagrams of the Au₃Cu-, AuCu-, and AuCu₃-type sublattice systems, as well as Au-Cu system. It means that all alloy phases share a set of $G_i^{\text{Au}}(T)$ and $G_i^{\text{Cu}}(T)$ level sequences and other properties sequences.

4.2 Discussion on critical temperature

Many experimental results show that the order degree of order/disorder transition decreases slowly initially, then becoming more rapid until the so-called T_c-critical temperature is achieved, followed by a "tailing-off". The fact that the completion of the disordering process occurs slowly is borne out by the detection of short-range order at temperatures considerably above the so-called critical temperature [20,25]. Therefore, it was pointed out that the meaning of a critical temperature is at the best uncertainty in view of the results of the present experiment. However, since the term has had such venerable usage, and since a critical temperature can be defined from the results of long-range order studies, we have defined the "critical" temperature by an extrapolation of the relatively precipitous portion of the curves of S (order degree) versus temperature. No particular significance is attached to this, other than experimental uncertainty [21].

In the QMAC-thermodynamics and CALPHAD-thermodynamics, a particular significance is attached to the so-called critical temperature, which is considered the assessed T_c -critical temperature of the order–disorder equilibrium transition and the composition-dependent T_c -x curve is considered selected information about phase boundary of order–disorder equilibrium transition for fitting the parameters in the Gibbs energy functions to achieve the best representation of the selected information. Therefore, the phase diagram

calculated in this way not only is not real equilibrium but goes so far to be erroneous (see Appendix A.1).

In the AGA-thermodynamics, the T_c -critical temperature is defined as the beginning temperature of perfect disordering during the equilibrium order-disorder transition, which may be obtained by the cross point of the $\Delta G_{\min}^{m} - T$ and $\Delta G_{\sigma=0}^{m} - T$ curves of ordered and disordered phase for a given compositional alloy in the solid Au-Cu system. The composition-dependent T_c -xcurve for a given ordered sublattice system is defined as the phase boundary curve between the ordered and disordered phases, which may be obtained by the equilibrium mixed Gibbs energy path method of alloys or by the difference method of Gibbs energies between the ordered and disordered phases, and the experimental so-called T_c-critical temperature is called as the T_i-jumping temperature arisen from existing critical σ_i -jumping order degree(see Appendix A.2). The all experimental T_i -values fall within the 0.60 $<\sigma<0.85$ region in Figs. 3(c) and (d), which are dependent on heating rate and composition of alloys (see Appendix A.3).

4.3 Discussion on subequilibrium statistic region-scale heterogeneity

Up to now, researchers have got used to recognizing the experimental phenomena observed during very slow variation in temperature to be thermodynamic equilibrium, and then treating experimental phenomena by equilibrium theory and method, lacking a real equilibrium theory and a standard path of order-disorder transition. For example, the order-disorder transition in Au-Cu alloys containing 65.8%-84.5%Cu (atomic fraction) was accomplished by observing high-angle fundamental X-ray reflections from single crystals, at temperatures ranging from room temperature to 450 °C (723 K). The conclusions indicate that the transition is a classical phase change with ordered and disordered phases presented in equilibrium for alloys containing less than 75% Cu, and the equilibrium diagram would show the ordered phase separated from the disordered phase by a two-phase region [21].

According to the essential definition of equilibrium order–disorder transition(see Section 3.1), there is no coexisting temperature range of ordered and disordered phases, during the equilibrium transition process for a given compositional alloy, which may be proved by the iso-order degree (or isothermal) Gibbs energy equilibrium path method (see Fig. 1) [29]. In the equilibrium phase diagrams of the Au₃Cu-type, AuCu-type and AuCu₃-type sublattice systems, there is no two-phase region of ordered and disordered phases with different compositions, which may be proved by the difference method of Gibbs energies between ordered

and disordered phases (see Appendix A.3).

In the AGA-subequilibrium thermodynamics, the essential definition of subequilibrium order—disorder transition is that the AG-Gibbs energy levels can respond immediately with each small variation in temperature, but the AG-probabilities (concentrations) occupied at the AG-Gibbs energy levels cannot change synchronously, even by extremely heating rate, which leads to its Gibbs energy path higher than that of equilibrium path. This transition needs the RA-SA atom movement mechanism together with superheated driving Gibbs energy [28].

Taking experimental path on disordering AuCuI $(A_8^{\text{Au}}A_4^{\text{Cu}})$ composed of A_8^{Au} and A_4^{Cu} stem alloy genes as an example, we presented three discoveries [28]: 1) The ability of AuCuI $(A_8^{\text{Au}}A_4^{\text{Cu}})$ to keep structure stabilization against changing temperature is attributed to the fact that the A_8^{Au} and A_4^{Cu} potential well depths greatly surpass their vibration energies, which leads to the subequilibrium of experimental path subequilibrium; 2) The RA-SA mechanism leads to heterogeneous and successive subequilibrium transitions; 3) There exist jumping alloy genes and jumping order degree, which lead to the existence of jumping T_i -temperature. The heterogeneous subequilibrium successive transitions on disordering stoichiometric AuCuI ($A_8^{Au}A_4^{Cu}$) by slow heating rate are as follows: AuCuI $(A_8^{Au}A_4^{Cu}) \rightarrow AuCu$ $(H)\rightarrow PTP-AuCu\rightarrow SPAP-AuCuII\rightarrow AuCu (L)\rightarrow AuCu$ (D), of which the kinetic behaviors are closely related to heating rates. When 0 K $\leq T \leq T_{\text{onset}}$, it is the unchanged period of the AuCuI ($A_8^{\text{Au}}A_4^{\text{Cu}}$). Its behaviors are as follows: 1) There exists no variation in order degree until $T_{\rm onset}$ (593K)-temperature is achieved. Namely, there exists no positional exchange between A_8^{Au} and A_4^{Cu} alloy genes, which are still occupied at the G_8^{Au} - and G_4^{Cu} - energy levels, respectively; 2) The superheated driving Gibbs energy $(\Delta G_{\min}^{m}(T) - \Delta G_{s}^{m}(T))$ between the equilibrium and subequilibrium paths increases with rising temperature, and their difference is -373 J/mol at 593 K, which is too small to exchange AG-positions; 3) The generalized vibration energies of A_8^{Au} and A_4^{Cu} alloy genes increase with rising temperature, but their values are much smaller than their potential well depths. At 593 K, the $U_8^{\text{Au.v}}/E_8^{\text{Au}}$ $\left|U_4^{\text{Cu.v}}/E_4^{\text{Cu}}\right|$ ratios are about 1/27! It means that only depending on superheated driving Gibbs energy and vibration energy, the $A_8^{\rm Au}$ and $A_4^{\rm Cu}$ alloy genes can not surmount potential barriers to alternate positions.

When $T_{\rm onset}$ (593 K)< $T \le 620$ K and $1.000 > \sigma_s \ge 0.990$, it is the growing period of the high order degree AuCu(H) alloy. During this period, there exists cell-scale (nucleation) heterogeneity in the growing period of the AuCu(H) alloy. Namely, the early-3(RA-SA) cell region with more 3(RA-SA) cells, middle-3(RA-SA) cells region with less 3(RA-SA) cells and late-AuCuI

 $(A_8^{\text{Au}}A_4^{\text{Cu}})$ cell region without 3(RA-SA) cell co-exist in the AuCu(H) alloy.

When 620 K< $T \le 650$ K and 0.990> $\sigma_s \ge 0.925$, it is the growing period of the statistic periodic antiphase (SPAP)-AuCuII region. During this period, there exists region-scale (nucleus growing) heterogeneity: the original early-3 (RA-SA) cell regions with more 3(RA-SA) cells grow into the early-(SPAP-AuCuII) regions, the original middle-3(RA-SA) cell regions with less 3(RA-SA) cells grow into the middle-(RA-SA) cell regions with more 3(RA-SA) cells and the original late-AuCuI ($A_8^{\text{Au}}A_4^{\text{Cu}}$) cell regions grow into the late-(RA-SA) cell regions with less 3(RA-SA) cells. Namely, the AuCu(H) region and SPAP-AuCuII region co-exist, and two distinct X-ray diffraction patterns may be observed at σ_s =0.925 [29]. This subequilibrium alloy with region-scale heterogeneity of order degrees is called as the pseudo-two-phases (PTP) AuCu alloy with the AuCu(H) regions and the SPAP-AuCuII regions. The use of the phrase "PTP" is intended to convey the impression that they are two heterogeneous subequilibrium regions with the same composition, different order degrees, and belong to the ordered AuCu-type sublattice phase, rather than coexisting ordered (σ >0) and disordered (σ =0) phases. It should be emphasized that: 1) This situation occurs at the high order degree period; 2) The RA-SA mechanism is a short range atom movement mechanism; 3) The two phase transition of the ordered and disordered phases with different compositions needs a long range atom movement (diffusion) mechanism.

When 650 K<T<683 K and 0.925> $\sigma_{\rm s}$ >0.807, it is the mature period of the SPAP-AuCuII alloy. During this period, the AuCu(H) regions are transferred into the SPAP-AuCuII regions. Therefore, the SPAP-AuCuII alloy containing early-, middle- and late-SPAP-AuCuII regions periods is a statistic periodic antiphase structure stacking of incommensurate tetragonal cells containing more $A_8^{\rm Au}$ and $A_4^{\rm Cu}$ alloy genes and antiphase boundary $n({\rm RA-SA})$ cells containing less $A_8^{\rm Au}$ and $A_4^{\rm Cu}$ alloy genes along b axis. It has no strict long periodic cell. The number M of cells between two successive antiphase boundaries is only an average, which is about 5.

When $0.807 \ge \sigma_s \ge 0.786$, it is the jumping period of the SPAP-AuCuII alloy. In this period, there are the maximum concentration emergent phenomena of jumping alloy genes associated with jumping order degrees of the alloy.

At the jumping temperature T_j =683 K, the SPAP-AuCuII alloy with high order degree (σ_j =0.807) jumps into the AuCu(L) alloy with low order degree (σ =0.4545). After the T_j -temperature, the AuCu(L) alloy is continuously transformed into the disordered AuCu (D)

alloy.

This example is enough to demonstrate that the "subequilibrium" statistic region-scale heterogeneity with the same composition and different order degrees has been erroneously considered as the heterogeneous "equilibrium" two-phase region of ordered (σ >0) and disordered (σ =0) phases with different compositions.

5 Conclusions

- 1) Based on the AG-Gibbs energy sequences and AGA-Gibbs energy level model, the AG-Gibbs energy partition function of the fcc-based lattice Au–Cu system has been established, which is used to describe the systematic correlativity of the AG-Gibbs energy levels, AG-probabilities occupied at the AG-Gibbs energy levels and degeneracy factor as functions of composition, temperature and order degree. This function may be suitable for AuCu-, AuCu₃- and Au₃Cu-type sublattice systems (σ >0), as well as disordered phase (σ =0) and other subequilibrium phases. However, their order degree definitions are different.
- 2) Based on the AG-holographic information database and essential definition of equilibrium order-disorder transition, the EHNP-diagrams of the AuCu₃-type sublattice have been established by the minimal mixed Gibbs energy path method. These diagrams exhibit unexpected characteristics equilibrium transition of AuCu₃-type sublattice system, and may be used as a standard for studying experimental subequilibrium transition. Once one network point has been clicked, the information about the composition, temperature, AG-concentrations, holographic properties and EHNP-charts of the alloy may be readily obtained. These achievements will prove stimulating to materials engineers, and who may well find value in using it as a big information database for materials discovery, design, manufacture and application.
- 3) The Gibbs energy-phase boundary curve has been obtained by the difference method of Gibbs energies between ordered and disordered phases. By this method, it has been proved that there is no two-phase region of ordered and disordered phases in the fcc-based lattice Au-Cu system.
- 4) Up to now, the researchers in the QMAC- and CALPHAD-communities have still taken erroneous understanding of experimental phenomena of order-disorder transition as the selected information, then established so-called Gibbs energy functions of ordered and disordered phases and so-called equilibrium phase diagram to achieve the best representation of the selected information. Since this way has had such venerable usage, it may be the biggest barrier hindering progress of the metal materials science and engineering.

Appendixes

A: Phase diagrams of Au-Cu system

A.1 Calculated phase diagrams of Au–Cu system by CALPHAD- and QMAC-thermodynamics

Before the present work, researchers have got used to recognizing the experimental phenomena observed during very slow variation in temperature to be thermodynamic equilibrium phenomena: 1) The middle jumping T_i -temperature is erroneously considered as the terminal T_c-critical temperature of order-disorder equilibrium transition of the alloy, although the experimental jumping σ_i -order degree is 0.8–0.7, and the experimental short range order degree exists at the temperatures considerablely above the T_i -temperature; 2) The composition-dependent $T_i(x)$ -points are erroneously considered the phase boundary points of phase diagram the AuCu₃-type sublattice system; 3) heterogeneous subequilibrium statistic region-scale heterogeneity with the same composition and different order degrees is erroneously considered as two heterogeneous equilibrium two-phase region consisting of ordered and disordered phases; 4) They hold that the stoichiometric Au₃Cu-, AuCu- and AuCu₃- compounds in the Au₃Cu-, AuCu- and AuCu₃-type sublattice systems have the lowest potential energies at 0 K and the highest $T_{\rm c}$ -critical temperatures on their phase boundary curves, respectively. The researchers in the QMAC- and **CALPHAD-communities** took these understandings of experimental phenomena as the selected information, then adjusted parameters in Gibbs energy functions and established so-called equilibrium phase diagrams to achieve the best representation of the selected information [19]. These phase diagrams are questionable in following respects (see Fig.A.1): 1) The so-called equilibrium phase boundary curve represents experimental subequilibrium T_i-jumping temperatures, not the real equilibrium T_c -critical temperatures; 2) There exists two-phase region of the ordered and disordered phases; 3) The compositions of the highest critical points of the Au₃Cu-, AuCu- and AuCu₃-sublattice systems are located the stoichiometric compositions: 25%Cu, 50%Cu 75%Cu (atomic fraction), respectively.

A.2 Jumping order degree

The σ_j -jumping order degree is defined as that the disordering begins to translate from a single splitting of the stem alloy genes to a universal splitting of the stem and jumping alloy genes.

In the AuCu₃-type sublattice system, the main jumping alloy genes of the AuCu₃ $(A_{12}^{\rm Au}(A_8^{\rm Cu})_3)$ compound consisting of the $A_{12}^{\rm Au}$ and $3A_8^{\rm Cu}$ stem alloy genes are respectively the $A_{11}^{\rm Au}$, $A_7^{\rm Cu}$ and $A_9^{\rm Cu}$

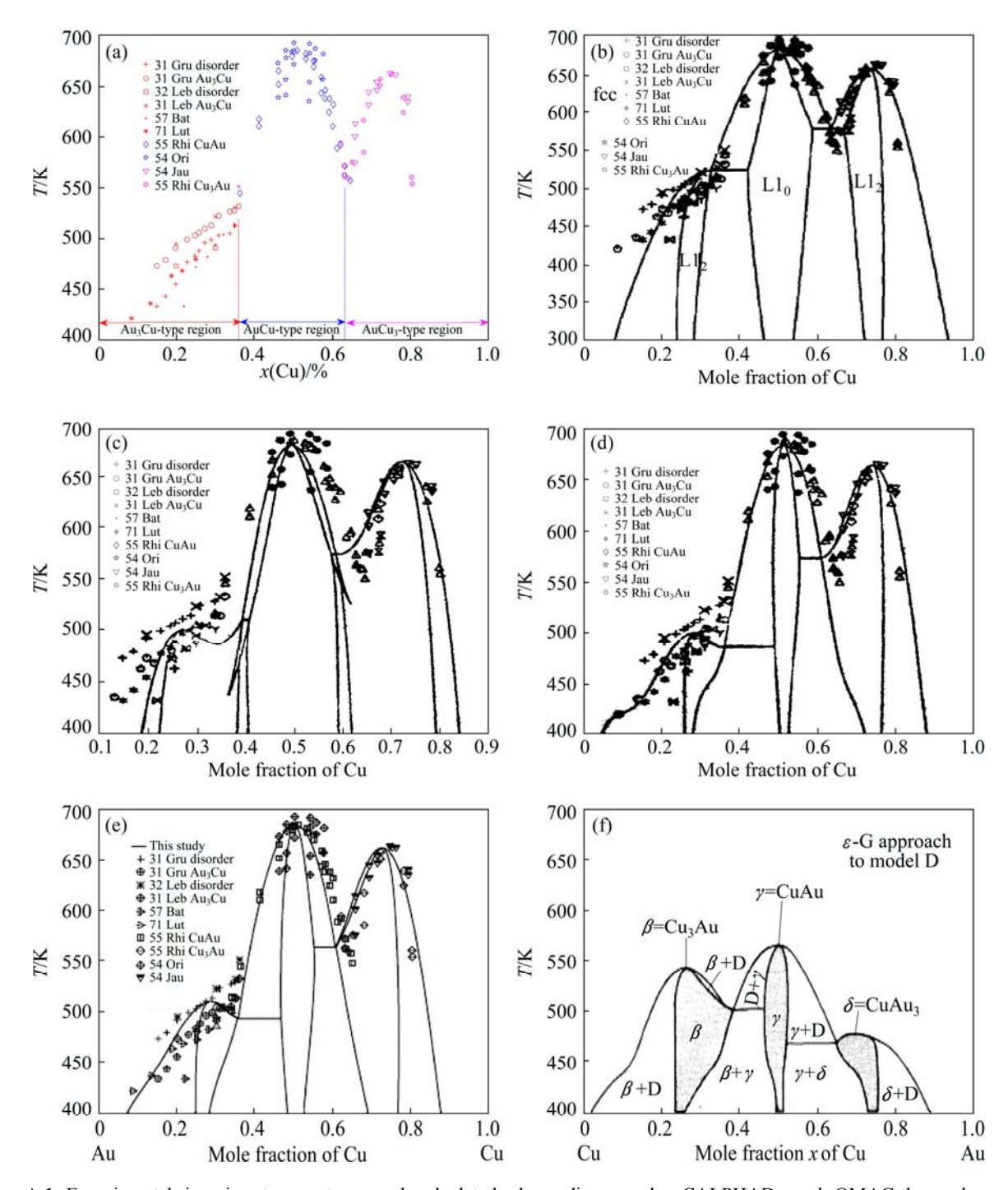


Fig. A.1 Experimental jumping temperatures and calculated phase diagrams by CALPHAD- and QMAC-thermodynamics: (a) Experimental jumping T_j -temperatures erroneously considered as equilibrium critical T_c -temperatures from in Ref. [14]; (b) Calculated Au–Cu phase diagram from Ref. [15]; (d) Calculated Au–Cu phase diagrams from Ref. [15]; (e) Calculated Au–Cu phase diagrams from Ref. [36]; (f) Calculated Au–Cu phase diagrams from Ref. [37]

alloy genes; their $\sigma_{\rm j}$ -jumping order degrees with the maximum emergent concentrations are respectively $\sigma_{11,\rm j}^{\rm Au}$ =0.736, $\sigma_{7,\rm j}^{\rm Cu}$ = 0.755 and $\sigma_{9,\rm j}^{\rm Cu}$ =0.690; their maximum emergent concentrations are respectively $x_{11,\rm j}^{\rm Au}-x_{11,\rm dis}^{\rm Au}$ = 4.399%, $x_{7,\rm j}^{\rm Cu}-x_{7,\rm dis}^{\rm Cu}$ =4.211% and $x_{9,\rm j}^{\rm Cu}-x_{9,\rm dis}^{\rm Cu}$ =1.127%. These results have been shown in

Figs. A.2 (a) and (b).

In the AuCu-type sublattice system, the main jumping alloy genes of the AuCu ($A_8^{\text{Au}}A_4^{\text{Cu}}$) compound consisting of the A_8^{Au} and A_4^{Cu} stem alloy genes are respectively the A_7^{Au} , A_9^{Au} , A_3^{Cu} and A_5^{Cu} alloy genes; their σ_i -jumping order degrees with the maximum

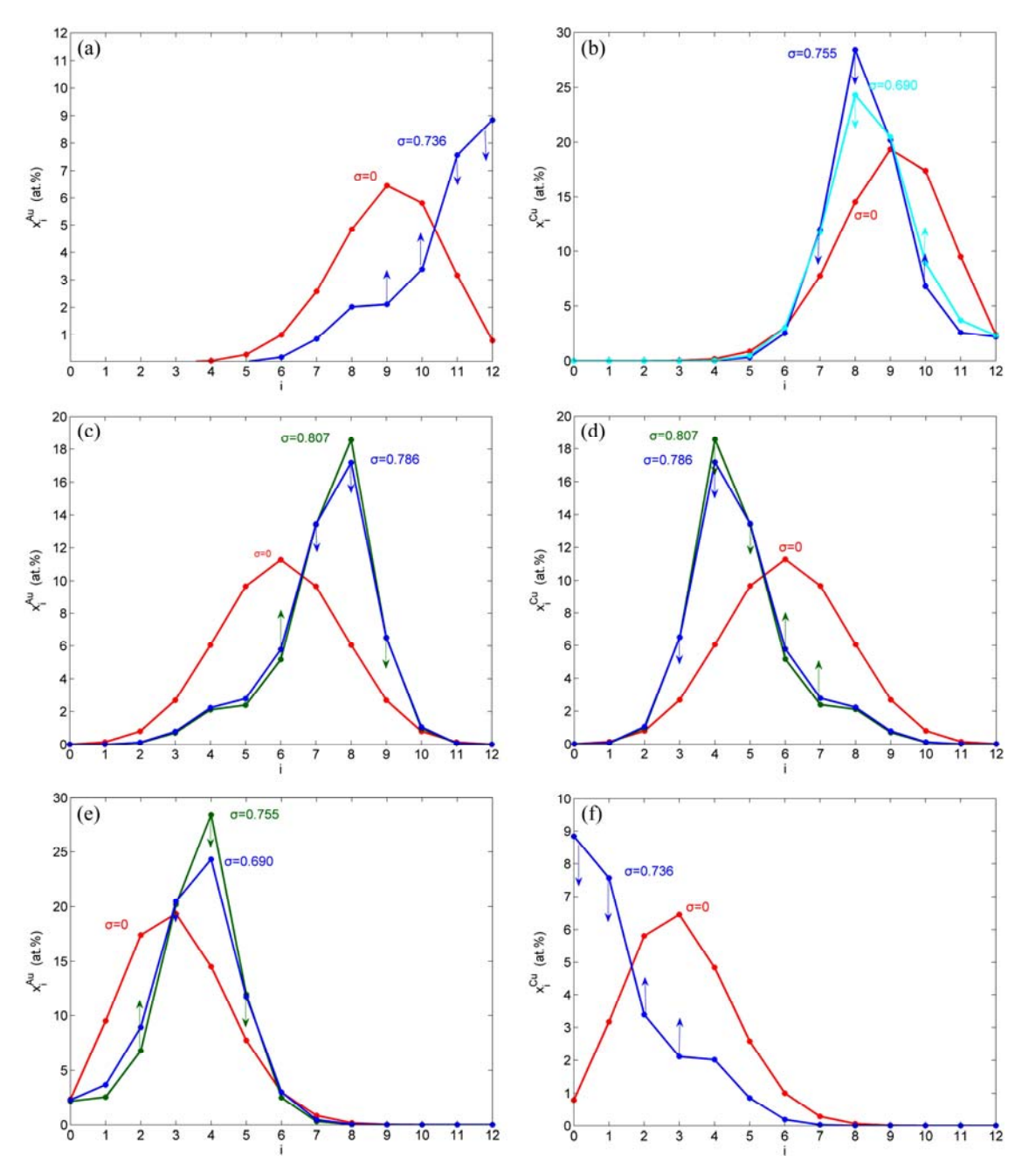


Fig. A.2 Main jumping alloy genes and their jumping order degrees: (a, b) Main jumping alloy genes (A_{11}^{Au} , A_{7}^{Cu} , A_{9}^{Cu}) and their jumping order degrees ($\sigma_{11,j}^{Au}$, $\sigma_{7,j}^{Cu}$, $\sigma_{9,j}^{Cu}$) of AuCu₃(A_{12}^{Au} (A_{8}^{Cu})₃) compound; (c, d) Main jumping alloy genes (A_{7}^{Au} , A_{9}^{Au} , A_{9}^{Au} , A_{3}^{Cu} , A_{5}^{Cu}) and their jumping order degrees ($\sigma_{7,j}^{Au}$, $\sigma_{9,j}^{Au}$, $\sigma_{3,j}^{Cu}$, $\sigma_{5,j}^{Cu}$) of AuCu($A_{8}^{Au}A_{4}^{Cu}$) compound; (e, f) Main jumping alloy genes (A_{3}^{Au} , A_{5}^{Au} , A_{5}^{Au} , A_{1}^{Cu}) and their jumping order degrees ($\sigma_{3,j}^{Au}$, $\sigma_{5,j}^{Au}$, $\sigma_{1,j}^{Cu}$) of Au₃Cu ((A_{4}^{Au})₃ A_{0}^{Cu}) compound

emergent concentrations are respectively $\sigma_{7,j}^{\text{Au}} = \sigma_{5,j}^{\text{Cu}} = 0.786$, $\sigma_{9,j}^{\text{Au}} = \sigma_{3,j}^{\text{Cu}} = 0.807$; their maximum emergent concentrations are respectively $x_{7,j}^{\text{Au}} - x_{7,\text{dis}}^{\text{Au}} = x_{5,j}^{\text{Cu}} - x_{5,\text{dis}}^{\text{Cu}} = 3.744\%$, $x_{9,j}^{\text{Au}} - x_{9,\text{dis}}^{\text{Au}} = x_{3,j}^{\text{Cu}} - x_{3,\text{dis}}^{\text{Cu}} = 3.800\%$. These results have been shown in Figs. A.2 (c) and (d).

In the Au₃Cu-type sublattice system, the main jumping alloy genes of the Au₃Cu($(A_4^{\text{Au}})_3 A_0^{\text{Cu}}$) compound consisted of the $3 A_4^{\text{Au}}$ and A_0^{Cu} stem alloy genes are respectively the A_3^{Au} , A_5^{Au} and A_1^{Cu} alloy genes; their σ_i -jumping order degrees with the

maximum emergent concentrations are respectively $\sigma_{3,j}^{\text{Au}}$ =0.690, $\sigma_{5,j}^{\text{Au}}$ =0.755 and $\sigma_{1,j}^{\text{Cu}}$ =0.736; their maximum emergent concentrations are respectively $x_{3,j}^{\text{Au}} - x_{3,\text{dis}}^{\text{Au}}$ =1.127%, $x_{5,j}^{\text{Au}} - x_{5,\text{dis}}^{\text{Au}}$ =4.211% and $x_{1,j}^{\text{Cu}} - x_{1,\text{dis}}^{\text{Cu}}$ =4.399%. These results have been shown in Figs. A.2 (e) and (f).

A.3 Jumping temperature

The T_j -jumping temperature is defined as the beginning split temperature of the jumping alloy genes. It is determined by the jumping order degree together with

superheated driving Gibbs energy. The completion of the disordering process occurs slowly by a "tailing-off" with short-range order at temperatures considerable above the T_j -jumping temperature. Therefore, it is the middle temperature of the subequilibrium order—disorder transition rather than the terminal T_c -critical temperature (see Fig. 1(c)).

A.4 Difference method of Gibbs energies between ordered and disordered phases

The $\Delta G_{\rm PB}^{\rm m}(x,T)$ - phase boundary curve of the AuCu₃-type sublattice system has been obtained by the difference method of Gibbs energies between ordered AuCu₃-type phase and disordered phase (see Fig. A.3). It has been proved that there is no two-phase region of the ordered and disordered phases, because ordered and disordered alloys belong to the same fcc-based lattice Au-Cu system.

B: EHNP charts of stoichiometric AuCu₃ alloy

According to $x_{i,e}^{\text{Au}} - T$ and $x_{i,e}^{\text{Cu}} - T$ paths on equilibrium order—disorder transition obtained by the minimal mixed Gibbs energy $\Delta G_{\min}^{\text{m}} - T$ method, the EHNP charts are calculated by Eqs. (5)–(8) and shown in

Figs.B.1 to B.14. By the same method, the systematic correlativity data of the $\Delta G_{\rm e}^{\rm m}(x,T)$, $\sigma_{\rm e}(x,T)$, $S^{\rm c}(x,T)$, $x_{i,\rm e}^{\rm Au}(x,T)$ and $x_{i,\rm e}^{\rm Cu}(x,T)$ on equilibrium order-disorder transition paths as function of composition and temperature for alloys of the AuCu₃-type sublattice system are calculated, using calculated steps Δx =0.5%, ΔT =1 K, $\Delta \sigma$ =0.0001.

C: other thermodynamic properties EHNP diagrams

According to $x_i^{\text{Au}} - x - T$ and $x_i^{\text{Cu}} - x - T$ EHNP diagrams obtained from $\Delta G^{\text{m}} - x - T$ diagram, we have obtained other q - x - T EHNP diagrams of AuCu₃-type sublattice system shown in Figs. C.1 to C.3. It should be emphasized that from each three-dimensional q - x - T EHNP diagram, we can obtain isocompositional $q_x - T$, isoproperty $T_q - x$ and isothermal $q_T - x$ path phase diagrams. These diagrams are interconnected to form a big database about structure, properties and their variations with temperature of alloy systems. Therefore, the knowledge of relationships of structure, properties and environments for alloy systems has been changed from single causality to systematic correlativity.

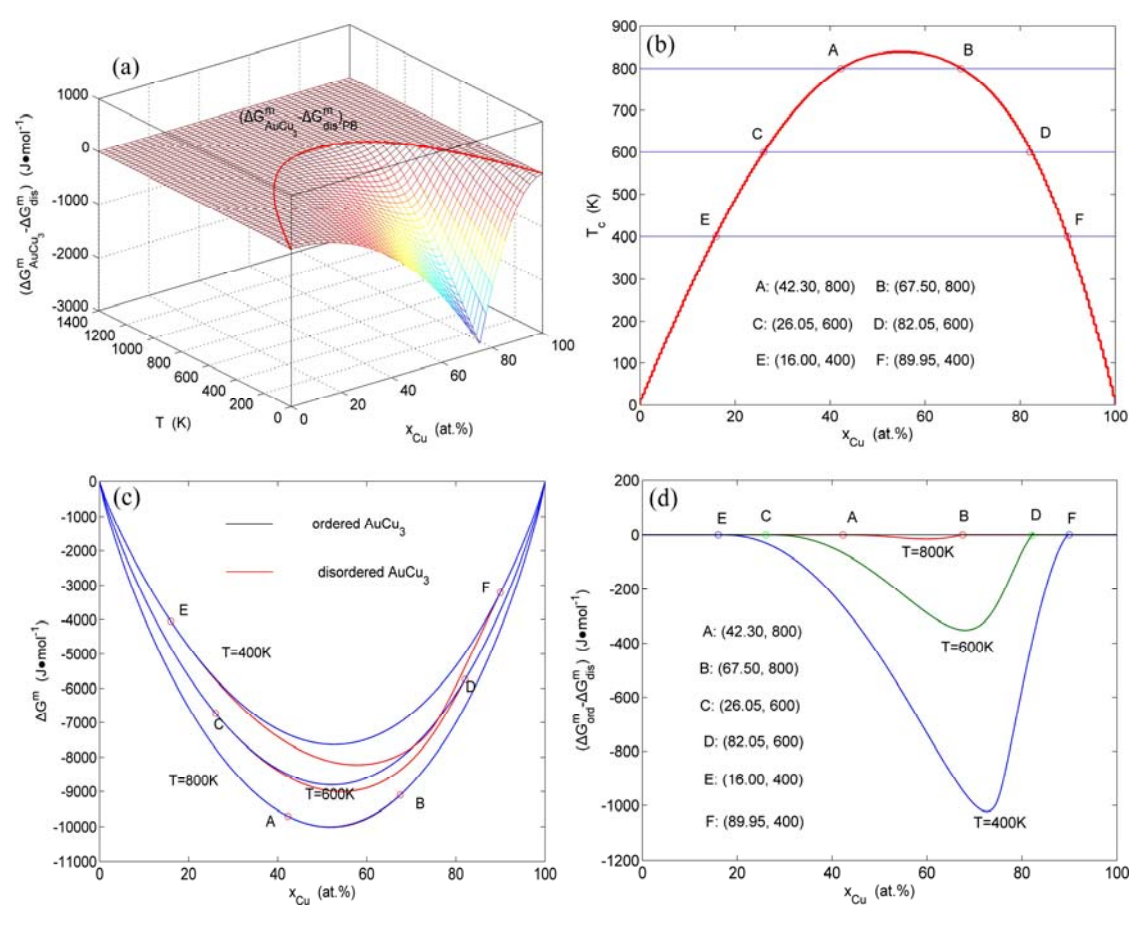


Fig. A.3 Difference method for calculating phase boundary curve of AuCu₃-type sublattice system: (a) Three-dimensional ($\Delta G_{\text{AuCu}_3}^{\text{m}} - \Delta G_{\text{dis}}^{\text{m}}$) diagram with phase boundary $\Delta G_{\text{PB}}^{\text{m}}(x,T)$ - curve; (b) Phase boundary $T_{\text{PB}}(x)$ - curve; (c) $\Delta G_{\text{ord}}^{\text{m}}$ - and $\Delta G_{\text{dis}}^{\text{m}}$ - curves at 400, 600 and 800 K as a function of composition; (d) Difference values of $\Delta G_{\text{ord}}^{\text{m}} - \Delta G_{\text{dis}}^{\text{m}}$ at 400, 600 and 800 K as a function of composition

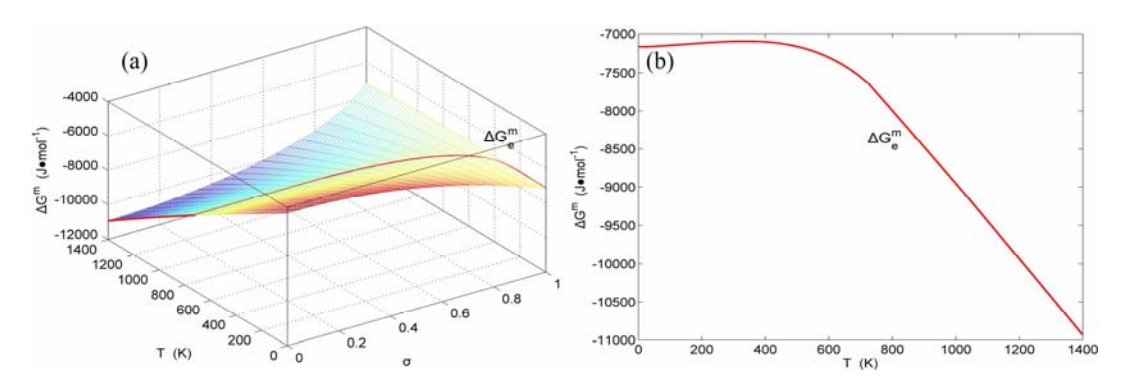


Fig. B.1 EHNP charts with EHNP curve of first order thermodynamic properties on disordering AuCu₃($A_{12}^{\text{Au}}(A_8^{\text{Cu}})_3$): (a) Three-dimensional mixed Gibbs energy $\Delta G^{\text{m}} - T - \sigma$ EHNP chart with $\Delta G_{\text{e}}^{\text{m}} - T$ paths; (b) $\Delta G_{\text{e}}^{\text{m}} - T$ path

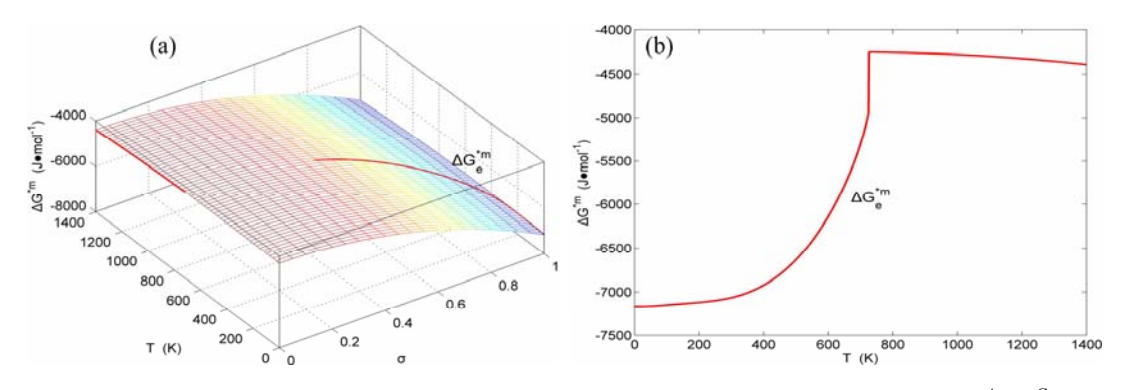


Fig. B.2 EHNP charts with EHNP curve of first order thermodynamic properties on disordering $\operatorname{AuCu_3}(A_{12}^{\operatorname{Au}}(A_8^{\operatorname{Cu}})_3)$: (a) Three-dimensional mixed characteristic Gibbs energy $\Delta G^{*m} - T - \sigma$ EHNP chart with $\Delta G_e^{*m} - T$ path; (b) $\Delta G_e^{*m} - T$ path

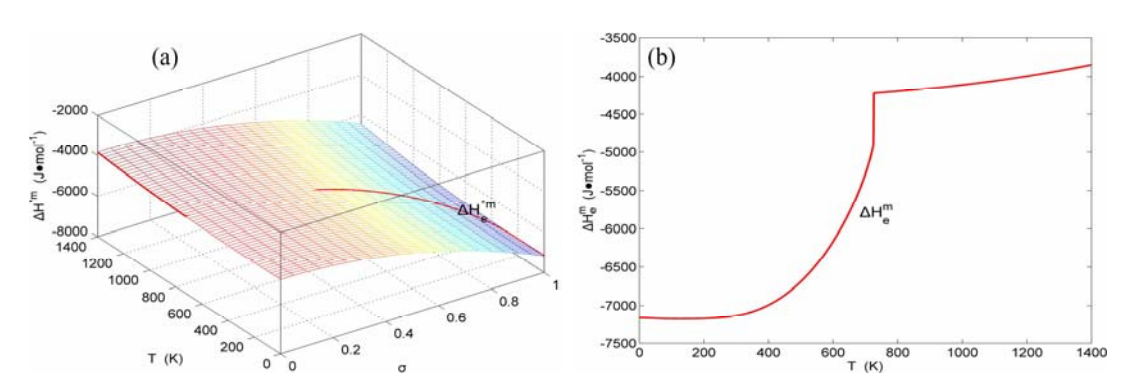


Fig. B.3 EHNP charts with EHNP curve of first order thermodynamic properties on disordering AuCu₃($A_{12}^{\text{Au}}(A_8^{\text{Cu}})_3$): (a) Three-dimensional mixed enthalpy $\Delta H^{\text{m}} - T - \sigma$ EHNP chart with $\Delta H_e^{\text{m}} - T$ path; (b) $\Delta H_e^{\text{m}} - T$ path

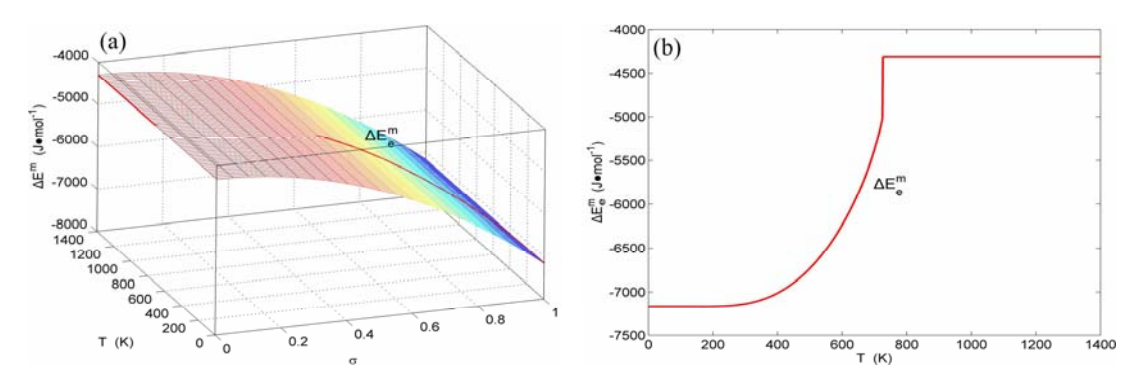


Fig. B.4 EHNP charts with EHNP curve of first order thermodynamic properties on disordering AuCu₃($A_{12}^{\text{Au}}(A_8^{\text{Cu}})_3$): (a) Three-dimensional mixed potential energy $\Delta E^{\text{m}} - T - \sigma$ EHNP chart with $\Delta E_e^{\text{m}} - T$ path; (b) $\Delta E_e^{\text{m}} - T$ path

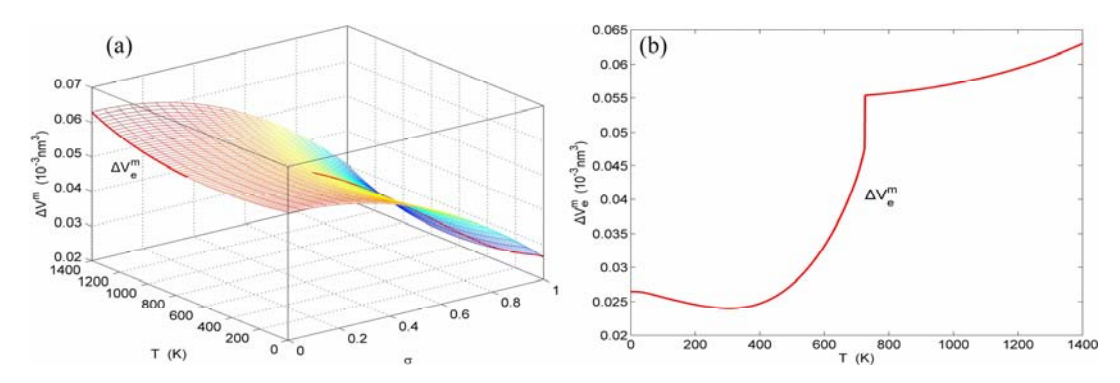


Fig. B.5 EHNP charts with EHNP curve of first order thermodynamic properties on disordering AuCu₃($A_{12}^{\text{Au}}(A_8^{\text{Cu}})_3$): (a) Three-dimensional mixed volume $\Delta V^{\text{m}} - T - \sigma$ EHNP chart with $\Delta V_{\text{e}}^{\text{m}} - T$ path; (b) $\Delta V_{\text{e}}^{\text{m}} - T$ path

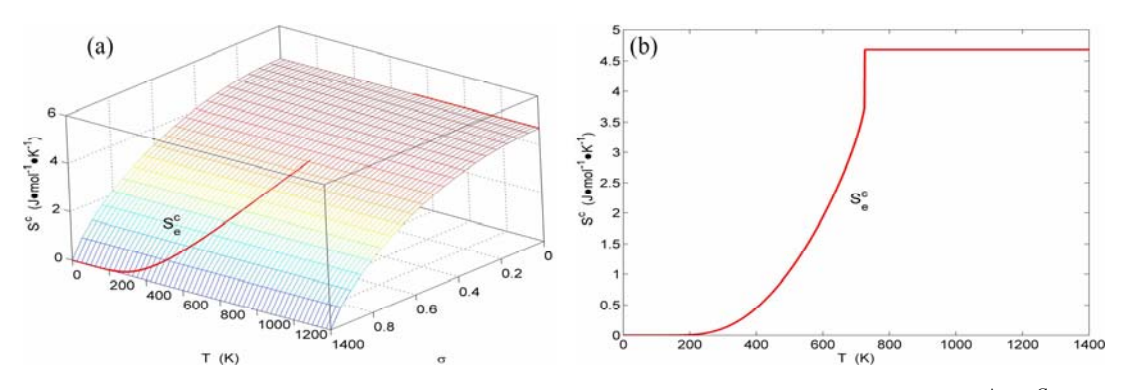


Fig. B.6 EHNP charts with EHNP curve of first order thermodynamic properties on disordering AuCu₃($A_{12}^{\text{Au}}(A_8^{\text{Cu}})_3$): (a) Three-dimensional configurational entropy $S^c - T - \sigma$ EHNP chart with $S_e^c - T$ path; (b) $S_e^c - T$ path

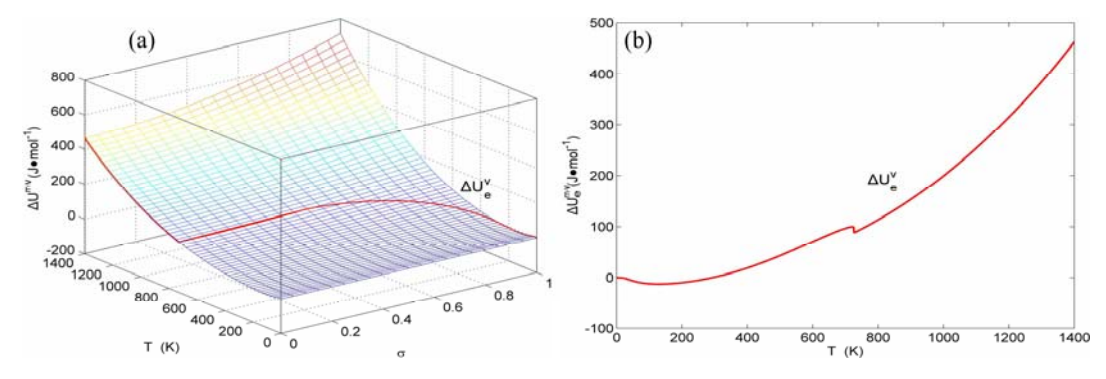


Fig. B.7 EHNP charts with EHNP curve of first order thermodynamic properties on disordering AuCu₃($A_{12}^{Au}(A_8^{Cu})_3$): (a) Three-dimensional generalized vibration energy $\Delta U^{m,v} - T - \sigma$ EHNP chart with $\Delta U_e^{m,v} - T$ path; (b) $\Delta U_e^{m,v} - T$ path

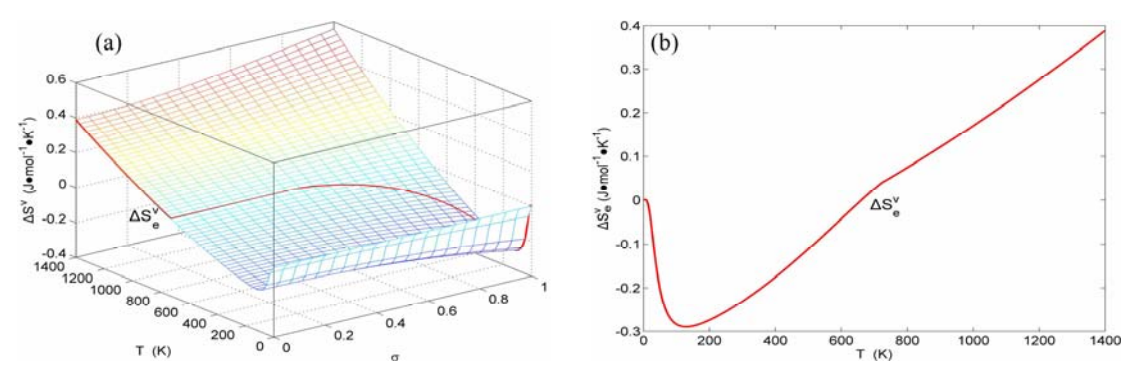


Fig. B.8 EHNP charts with EHNP curve of first order thermodynamic properties on disordering AuCu₃($A_{12}^{Au}(A_8^{Cu})_3$): (a) Three-dimensional generalized vibration entropy $\Delta S^v - T - \sigma$ EHNP chart with $\Delta S_e^v - T$ path; (b) $\Delta S_e^v - T$ path

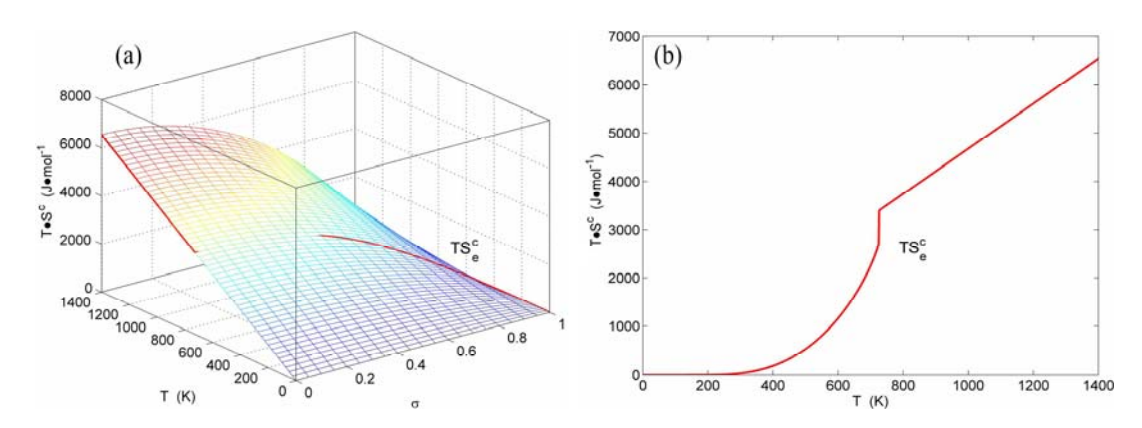


Fig. B.9 EHNP charts with EHNP curve of first order thermodynamic properties on disordering AuCu₃($A_{12}^{\text{Au}}(A_8^{\text{Cu}})_3$): (a) Three-dimensional configurational entropy energy $TS^c - T - \sigma$ EHNP chart with $TS_e^c - T$ path; (b) $TS_e^c - T$ path

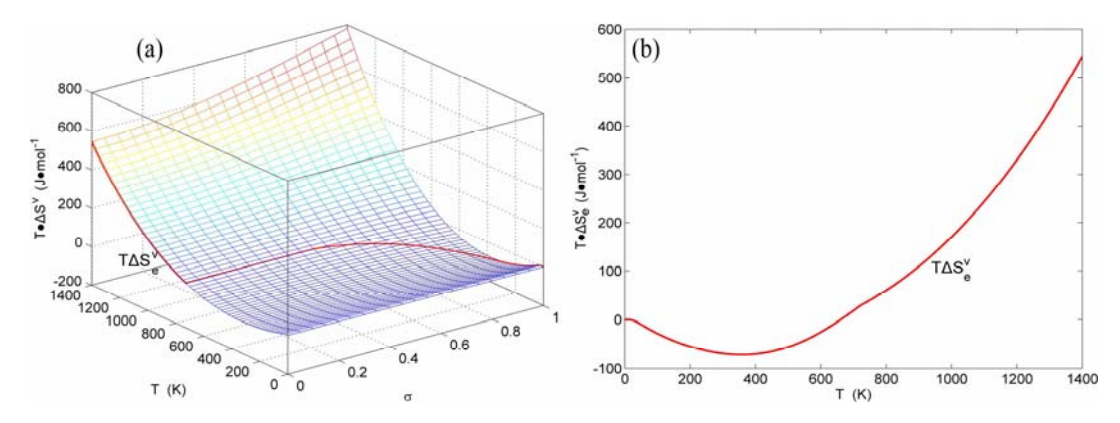


Fig. B.10 EHNP charts with EHNP curve of first order thermodynamic properties on disordering AuCu₃($A_{12}^{Au}(A_8^{Cu})_3$): (a) Three-dimensional generalized vibration entropy energy $T\Delta S^{\rm v} - T - \sigma$ EHNP chart with $T\Delta S_{\rm e}^{\rm v} - T$ path; (b) $T\Delta S_{\rm e}^{\rm v} - T$ path

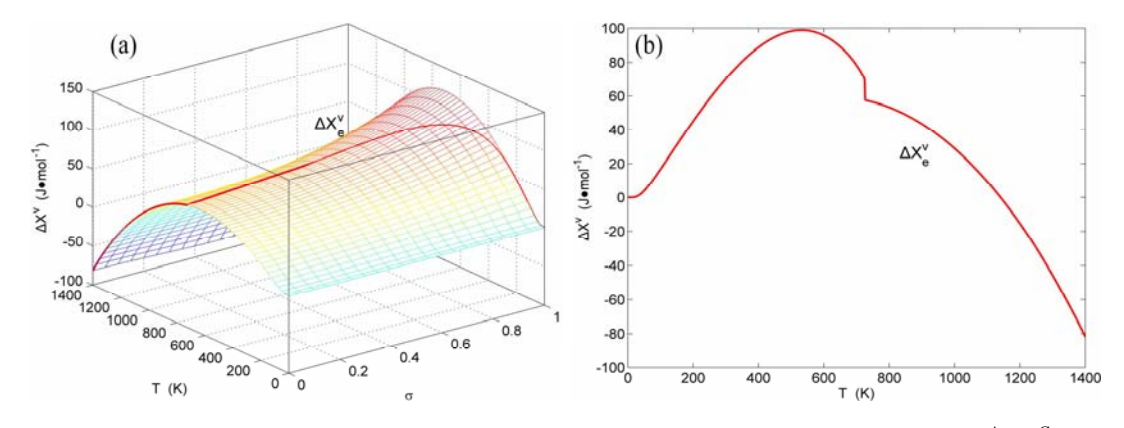


Fig. B.11 EHNP charts with EHNP curve of first order thermodynamic properties on disordering $\operatorname{AuCu_3}(A_{12}^{\operatorname{Au}}(A_8^{\operatorname{Cu}})_3)$: (a) Three-dimensional generalized vibration free energy $\Delta X^{\operatorname{v}} - T - \sigma$ EHNP chart with $\Delta X_{\operatorname{e}}^{\operatorname{v}} - T$ path; (b) $\Delta X_{\operatorname{e}}^{\operatorname{v}} - T$ path

D: AG-holographic information database of fcc-based lattice Au-Cu system

D.1 Thermodynamics properties of AG-sequences

In the SMMS framework, the characteristic Gibbs energy ($G_i(T)$) of each characteristic crystal (or alloy gene) may be split into two parts: a temperature-independent contribution of potential energy ($E_i(0)$), of

which the variation with temperatures has been accounted in the attaching vibration energy, and a temperature-dependent contribution of generalized vibration free energy ($X_i^{\rm v}(T)$), but both are energy level (*i*)-dependent (Eq. (1)). The enthalpy ($H_i(T)$) of each characteristic crystal may be also split into two parts: a temperature-independent contribution of potential energy

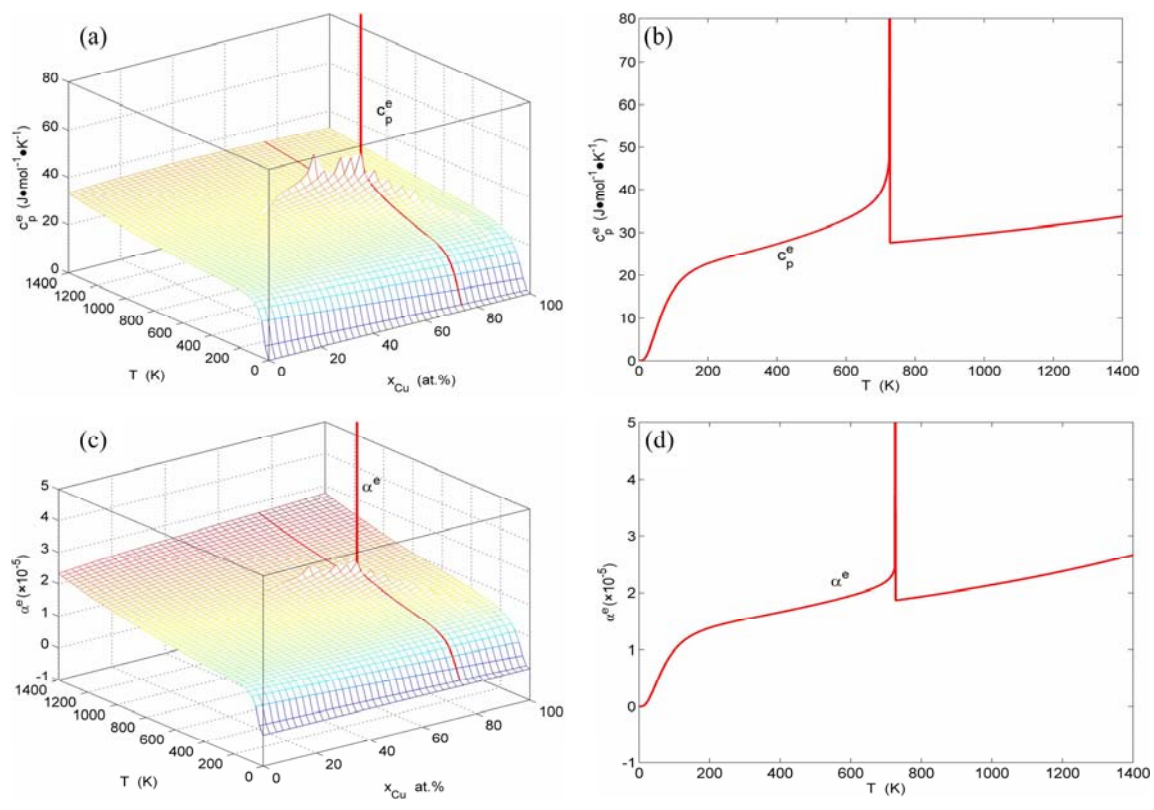


Fig. B.12 Second order thermodynamic properties (heat capacity and thermal expansion coefficient) on disordering AuCu₃ ($A_{12}^{\text{Au}}(A_8^{\text{Cu}})_3$): (a) $c_p^{\text{e}}-T$ path on c_p-x-T EHNP diagram; (b) $c_p^{\text{e}}-T$ path; (c) $\alpha^{\text{e}}-T$ path on $\alpha-x-T$ EHNP chart; (d) $\alpha^{\text{e}}-T$ path (These charts are calculated by the temperature step $\Delta T=1$ K and order degree step $\Delta\sigma=0.00001$)

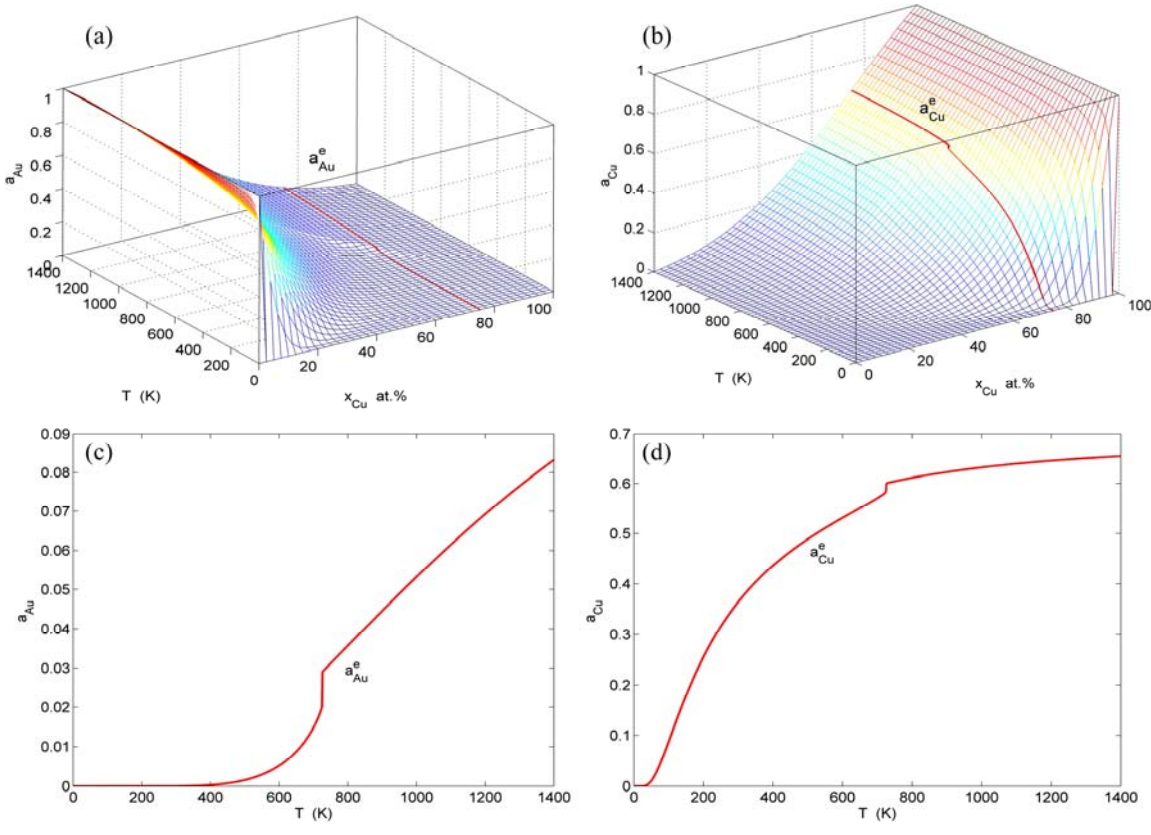


Fig. B.13 Activities on disordering AuCu₃ ($A_{12}^{Au}(A_8^{Cu})_3$): (a) $a_{Au}^e - T$ a path on $a_{Au} - x - T$ diagram; (b) $a_{Cu}^e - T$ path on $a_{Cu} - x - T$ EHNP diagram; (c) $a_{Au}^e - T$; (d) $a_{Cu}^e - T$ path

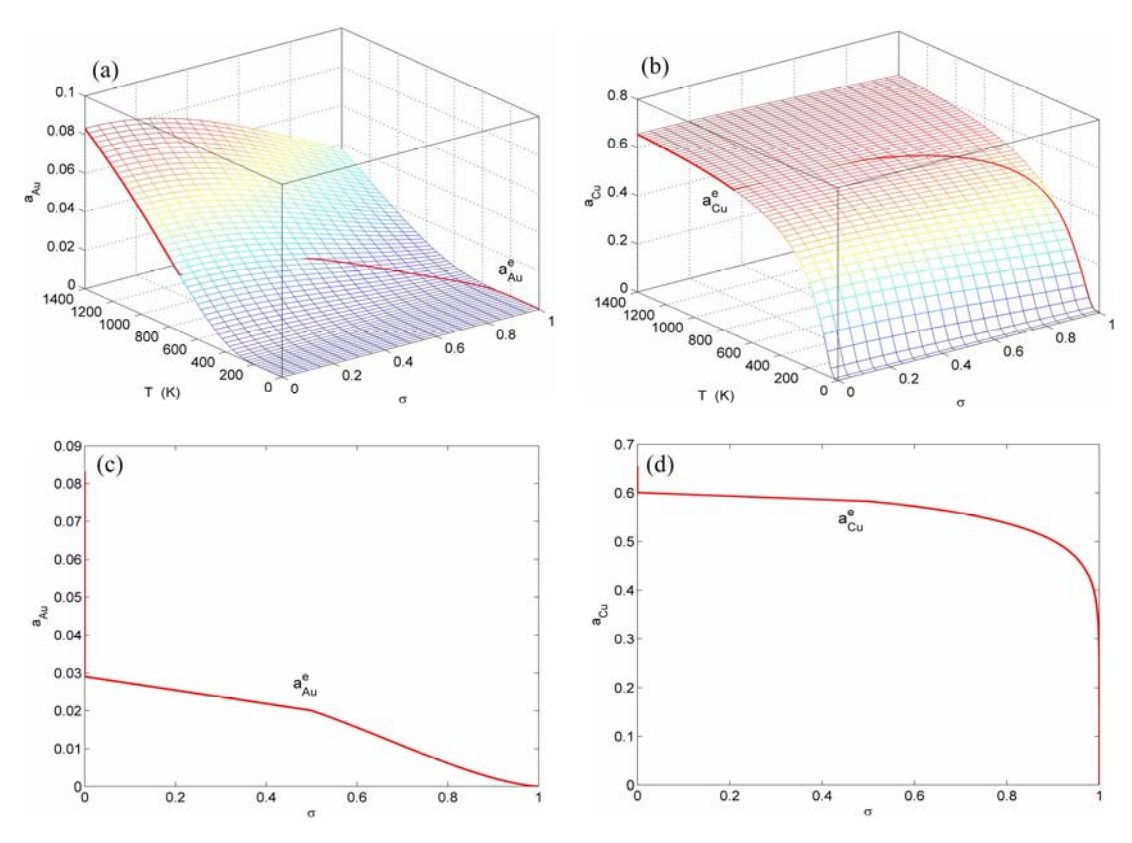


Fig. B.14 Activities on disordering AuCu₃ ($A_8^{\rm Au}(A_8^{\rm Cu})_3$): (a) $a_{\rm Au}^{\rm e}-T$ path on $a_{\rm Au}-T-\sigma$ EHNP chart; (b) $a_{\rm Cu}^{\rm e}-T$ and $a_{\rm Cu}-T-\sigma$ EHNP chart; (c) $a_{\rm Au}^{\rm e}-\sigma$; (d) $a_{\rm Cu}^{\rm e}-\sigma$ path

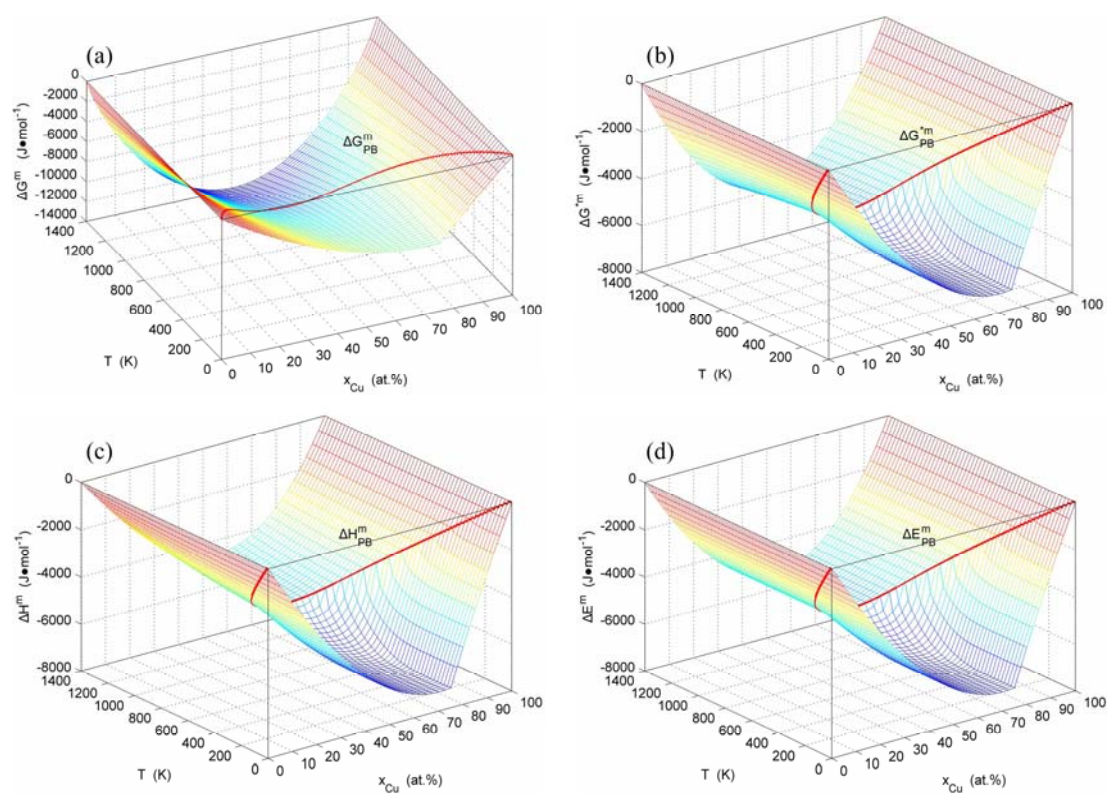


Fig. C.1 q-x-T EHNP diagrams of AuCu₃-type sublattice system: (a) Mixed Gibbs energy $\Delta G^m - x - T$ three-dimensional EHNP diagram; (b) Mixed characteristic Gibbs energy $\Delta G^{*m} - x - T$ three-dimensional EHNP diagram without configuration entropy; (c) Mixed enthalpy $\Delta H^m - x - T$ three-dimensional EHNP diagram; (d) Mixed potential energy $\Delta E^m - x - T$ three-dimensional EHNP diagram, without variations in AG-potential energies with temperatures

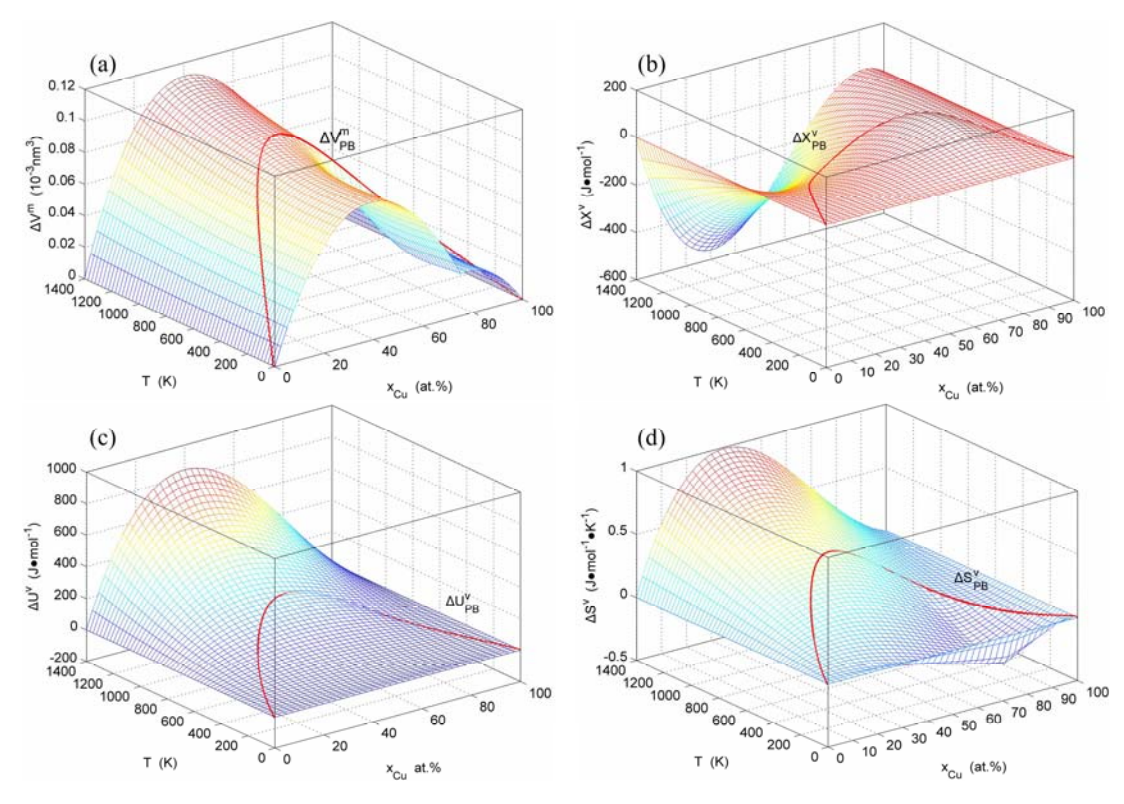


Fig. C.2 q-x-T EHNP diagrams of AuCu₃-type sublattice system: (a) Mixed volume $\Delta V^{\rm m} - x - T$ three-dimensional EHNP diagram; (b) Generalized mixed vibration free energy $\Delta X^{\rm v} - x - T$ three-dimensional EHNP diagram; (c) Generalized mixed vibration energy $\Delta U^{\rm v} - x - T$ three-dimensional EHNP diagram, including variations in AG-potential energies with temperatures; (d) Generalized mixed vibration entropy $\Delta S^{\rm v} - x - T$ three-dimensional EHNP diagram

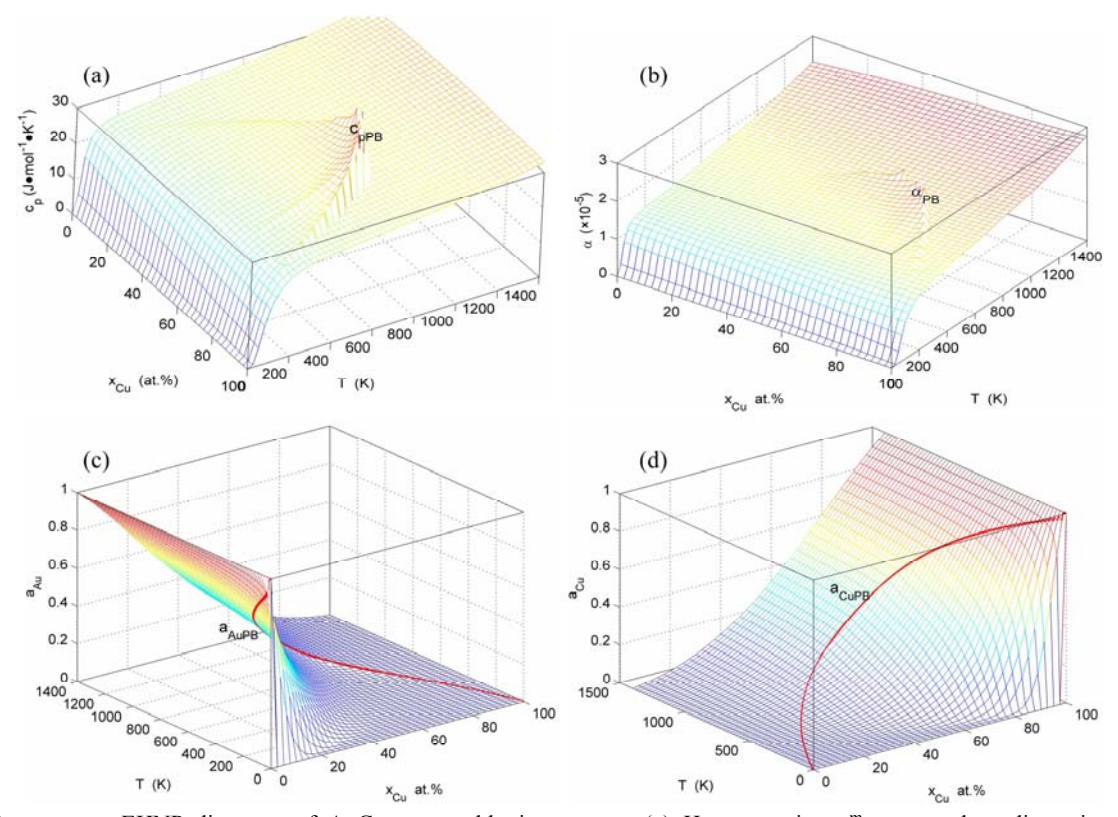


Fig. C.3 q-x-T EHNP diagrams of AuCu₃-type sublattice system: (a) Heat capacity $c_p^{\rm m}-x-T$ three-dimensional EHNP diagram; (b) Thermal expansion coefficient $\alpha-x-T$ three-dimensional EHNP diagram; (c) $a_{\rm Au}-x-T$ three-dimensional diagram; (d) $a_{\rm Cu}-x-T$ three-dimensional diagram

 $(E_i(0))$ and a temperature-dependent contribution of generalized vibration energy $(U_i^{v}(T))$ (Eq. (2)). The generalized vibration free energy includes the generalized vibration energies $(U_i^{\rm v}(T))$, which include Debye vibration energies ($U_i^D(T)$) and attaching vibration energies $(U_i^{\rm E}(T))$, the contribution of the generalized vibration entropies $(S_i^{v}(T))$ (Eq. (3)), which include Debye vibration entropies ($S_i^{D}(T)$) and attaching vibration entropies ($S_i^{E}(T)$), and the generalized vibration heat capacity ($c_{p,i}^{v}(T)$), which include Debye vibration heat capacity ($c_{p,i}^{\rm D}(T)$), attaching vibration heat capacity ($c_{p,i}^{\rm E}(T)$). The attaching vibration energy includes contributions of electron excitation, energy of formation of holes, variation of potential energy with temperature, and expansion work $(P\Delta V_i(T))$ of volume. Therefore, the multi-level energetic functions of characteristic crystals at TK are as follows:

$$\begin{cases} G_i^{\text{Au}}(T) = E_i^{\text{Au}}(0) + X_i^{\text{Au},\text{V}}(T) = H_i^{\text{Au}}(T) - TS_i^{\text{Au},\text{V}}(T) \\ G_i^{\text{Cu}}(T) = E_i^{\text{Cu}}(0) + X_i^{\text{Cu},\text{V}}(T) = H_i^{\text{Cu}}(T) - TS_i^{\text{Cu},\text{V}}(T) \end{cases}$$
(1)

$$\begin{cases} H_i^{\text{Au}}(T) = E_i^{\text{Au}}(0) + U_i^{\text{Au},\text{v}}(T) \\ H_i^{\text{Cu}}(T) = E_i^{\text{Cu}}(0) + U_i^{\text{Cu},\text{v}}(T) \end{cases}$$
(2)

$$\begin{cases} X_i^{\text{Au.v}}(T) = U_i^{\text{Au.v}}(T) - TS_i^{\text{Au.v}}(T) \\ X_i^{\text{Cu.v}}(T) = U_i^{\text{Cu.v}}(T) - TS_i^{\text{Cu.v}}(T) \end{cases}$$
(3)

$$\begin{cases} X_i^{\text{Au.v}}(T) = X_i^{\text{Au.D}}(T) + X_i^{\text{Au.E}}(T) \\ X_i^{\text{Cu.v}}(T) = X_i^{\text{Cu.D}}(T) + X_i^{\text{Cu.E}}(T) \end{cases}$$
(4)

$$\begin{cases} S_i^{\text{Au.v}}(T) = S_i^{\text{Au.D}}(T) + S_i^{\text{Au.E}}(T) \\ S_i^{\text{Cu.v}}(T) = S_i^{\text{Cu.D}}(T) + S_i^{\text{Cu.E}}(T) \end{cases}$$
(5)

$$\begin{cases} X_i^{\text{Au.D}}(T) = U_i^{\text{Au.D}}(T) - TS_i^{\text{Au.D}}(T) \\ X_i^{\text{Cu.D}}(T) = U_i^{\text{Cu.D}}(T) - TS_i^{\text{Cu.D}}(T) \end{cases}$$

$$(6)$$

$$\begin{cases} X_i^{\text{Au.E}}(T) = U_i^{\text{Au.E}}(T) - TS_i^{\text{Au.E}}(T) \\ X_i^{\text{Cu.E}}(T) = U_i^{\text{Cu.E}}(T) - TS_i^{\text{Cu.E}}(T) \end{cases}$$
(7)

$$\begin{cases} U_i^{\text{Au.v}}(T) = U_i^{\text{Au.D}}(T) + U_i^{\text{Au.E}}(T) \\ U_i^{\text{Cu.v}}(T) = U_i^{\text{Cu.D}}(T) + U_i^{\text{Cu.E}}(T) \end{cases}$$
(8)

$$\begin{cases} U_i^{\text{Au,D}}(T) = \int_0^T c_{p,i}^{\text{Au,D}}(T) dT \\ U_i^{\text{Cu,D}}(T) = \int_0^T c_{p,i}^{\text{Cu,D}}(T) dT \end{cases}$$

$$(9)$$

$$\begin{cases} S_{i}^{\text{Au.D}}(T) = \int_{0}^{T} \frac{c_{p,i}^{\text{Au.D}}(T)}{T} dT \\ S_{i}^{\text{Cu.D}}(T) = \int_{0}^{T} \frac{c_{p,i}^{\text{Cu.D}}(T)}{T} dT \end{cases}$$
(10)

$$\begin{cases} U_i^{\text{Au.E}}(T) = \int_0^T c_{p,i}^{\text{Au.E}}(T) dT \\ U_i^{\text{Cu.E}}(T) = \int_0^T c_{p,i}^{\text{Cu.E}}(T) dT \end{cases}$$
(11)

$$\begin{cases}
S_i^{\text{Au,D}}(T) = \int_0^T \frac{c_{p,i}^{\text{Au,D}}(T)}{T} dT \\
S_i^{\text{Cu,D}}(T) = \int_0^T \frac{c_{p,i}^{\text{Cu,D}}(T)}{T} dT
\end{cases}$$
(12)

$$\begin{cases} S_i^{\text{Au.E}}(T) = \int_0^T \frac{c_{p,i}^{\text{Au.E}}(T)}{T} dT \\ S_i^{\text{Cu.E}}(T) = \int_0^T \frac{c_{p,i}^{\text{Cu.E}}(T)}{T} dT \end{cases}$$
(13)

$$\begin{cases} \theta_{i}^{\text{Au}} = \theta_{0}^{\text{Au}} \times \sqrt{E_{i}^{\text{Au}}(0)/(V_{i}^{\text{Au}}(0))^{(2/3)}} / \\ \sqrt{E_{0}^{\text{Au}}(0)/(V_{0}^{\text{Au}}(0))^{(2/3)}} \\ \theta_{i}^{\text{Cu}} = \theta_{I}^{\text{Cu}} \times \sqrt{E_{i}^{\text{Cu}}(0)/(V_{i}^{\text{Cu}}(0))^{(2/3)}} / \\ \sqrt{E_{12}^{\text{Cu}}(0)/(V_{12}^{\text{Cu}}(0))^{(2/3)}} \end{cases}$$

$$(14)$$

$$\begin{cases} c_{p,i}^{\text{Au.D}}(T) = 9R \left(\frac{T}{\theta_i^{\text{Au}}}\right)^3 \int_0^{\theta_i^{\text{Au}}/T} \frac{e^x x^4}{(e^x - 1)^2} dx \\ c_{p,i}^{\text{Cu.D}}(T) = 9R \left(\frac{T}{\theta_i^{\text{Cu}}}\right)^3 \int_0^{\theta_i^{\text{Cu}}/T} \frac{e^x x^4}{(e^x - 1)^2} dx \end{cases}$$
(15)

$$\begin{cases} c_{p,0}^{\text{Au.E}}(T) = 1.858993 \times 10^{-10} T + 4.222584 \times 10^{-6} T^{2} \\ c_{p,12}^{\text{Au.E}}(T) = 2.763134 \times 10^{-4} T + 5.481502 \times 10^{-6} T^{2} \end{cases}$$
(16)

$$\begin{cases} c_{p,12}^{\text{Cu.E}}(T) = 0.00168035T + 2.826912 \times 10^{-6} T^2 \\ c_{p,0}^{\text{Cu.E}}(T) = 0.00564614T + 3.632353 \times 10^{-6} T^2 \end{cases}$$
 (17)

where
$$\theta_0^{Au}$$
 =165 K, θ_{12}^{Au} =175.21 K, θ_{12}^{Cu} =343 K, θ_0^{Cu} =343.07 K.

The valence electron structures (the number of free electrons $(s_{\rm f})$, covalent electrons $(S_{\rm c}, d_{\rm c})$ and non-valent electrons $(d_{\rm n})$, volumes (ν) , potential energies (ε) and single bond radii (R) of alloy genes, cohesive energy $(E_{\rm c})$, Debye temperatures (θ) and bulk moduli (B) of characteristic crystals have been obtained by the valence bond theory of characteristic crystals [27,38-40].

D.2 Flow chart for establishing AG-holographic information database of fcc-based Au-Cu system

The AG-holographic information database of the fcc-based Au–Cu system has been established by AG-theory, which is shown in Fig.D.1.

D.3 Figures of thermodynamics properties of AGsequences

The thermodynamics properties of AG-sequences are shown in Figs.D.2—D.4, which may be used to establish EHNP-diagrams of Au-Cu system.

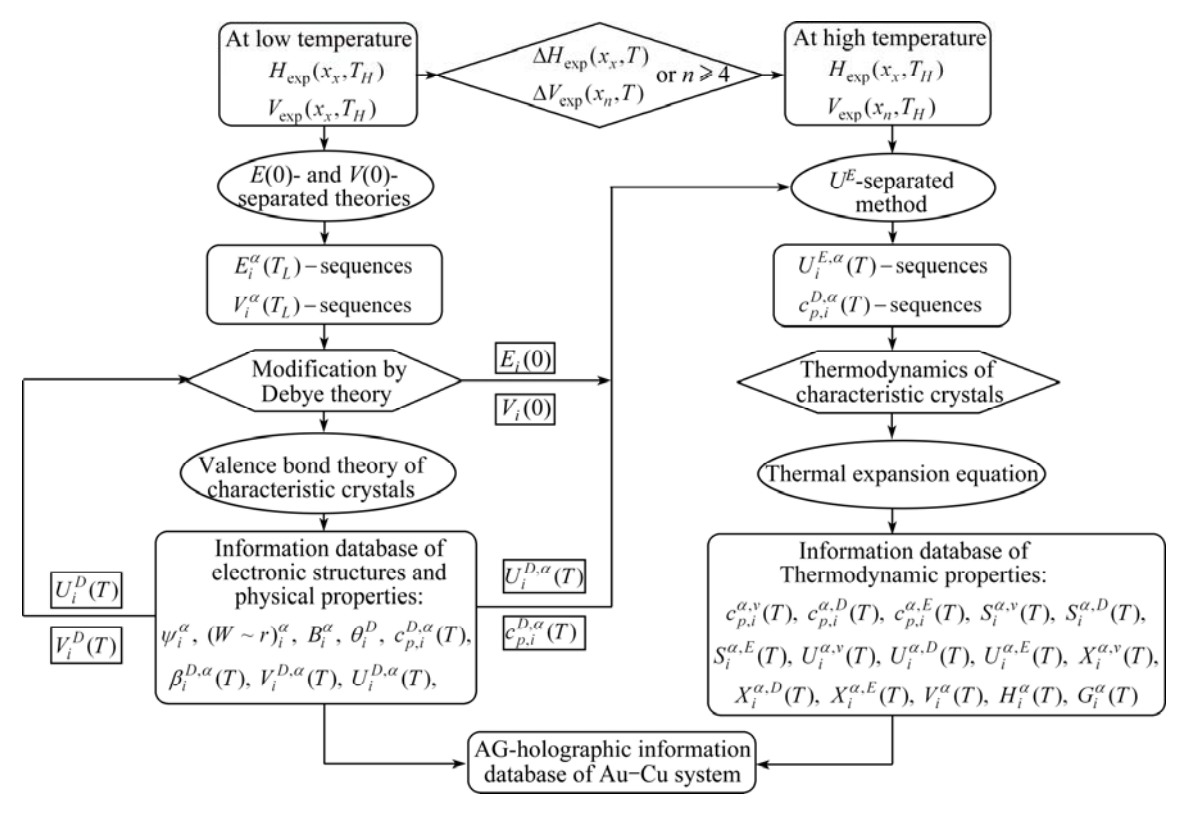


Fig. D.1 Flow chart for establishing AG-holographic information database of fcc-based Au-Cu system

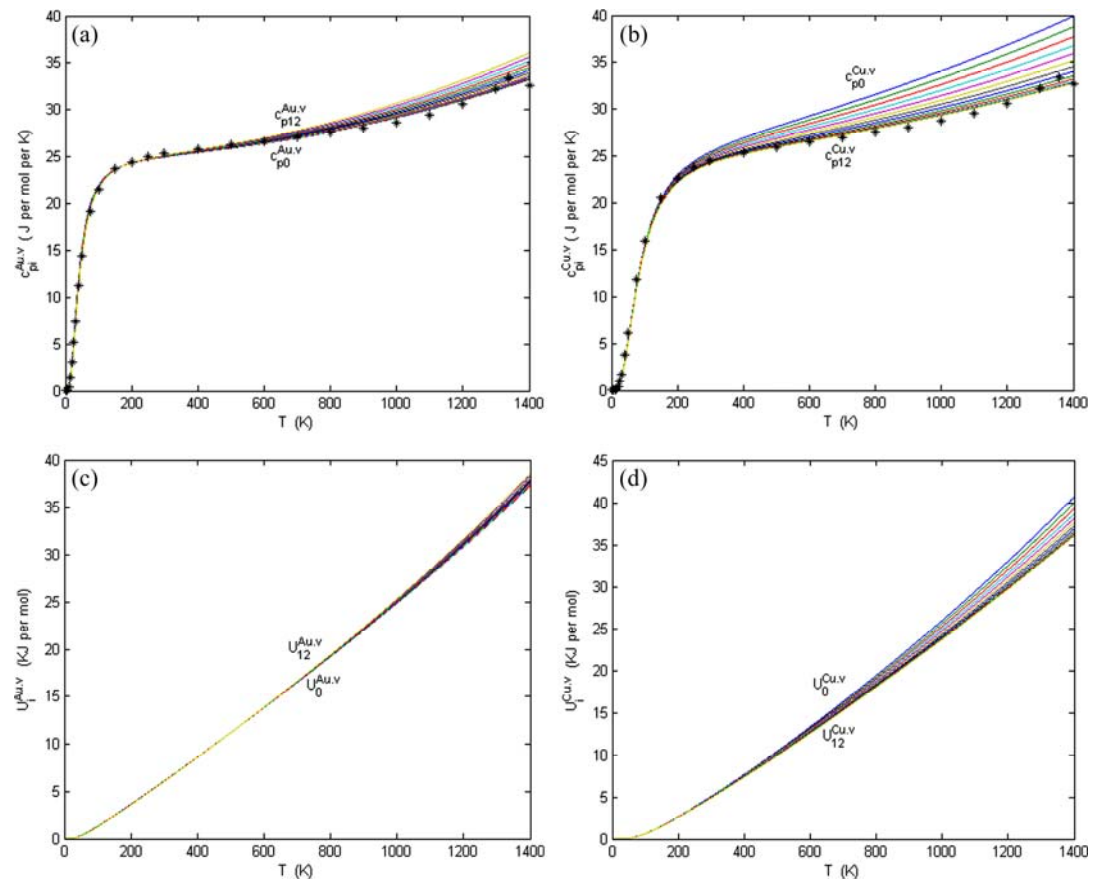


Fig. D.2 Curves of AG-thermodynamic properties in Au–Cu system: (a) Generalized vibration heat capacity levels: $c_{p,0}^{\text{Au.v}}, \cdots, c_{pi}^{\text{v.Au}}, \cdots, c_{pi2}^{\text{v.Au}}$; (b) Generalized vibration heat capacity levels: $c_{p,0}^{\text{Cu.v}}, \cdots, c_{p,i}^{\text{Cu.v}}, \cdots, c_{p,12}^{\text{Cu.v}}$; (c) Generalized vibration energy levels: $U_0^{\text{Au.v}}, \cdots, U_i^{\text{Cu.v}}, \cdots, U_i^{\text{Cu.v}}, \cdots, U_{i2}^{\text{Cu.v}}$; (d) Generalized vibration energy levels: $U_0^{\text{Cu.v}}, \cdots, U_i^{\text{Cu.v}}, \cdots, U_{i2}^{\text{Cu.v}}, \cdots, U_{i2}^{\text{Cu.v}}$

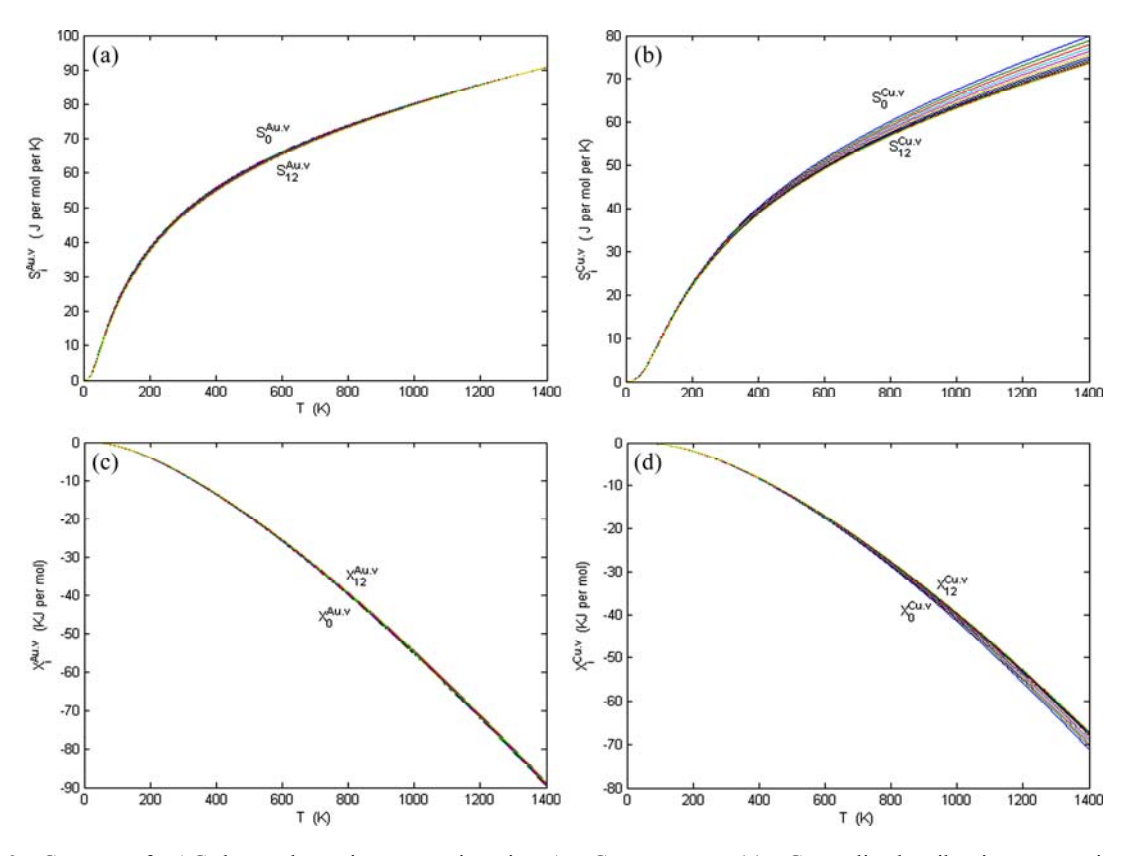


Fig. D.3 Curves of AG-thermodynamic properties in Au–Cu system: (a) Generalized vibration entropies levels: $S_0^{\text{Au.v}}, \cdots, S_i^{\text{Au.v}}, \cdots, S_{12}^{\text{Au.v}}$; (b) Generalized vibration entropies levels: $S_0^{\text{Cu.v}}, \cdots, S_i^{\text{Cu.v}}, \cdots, S_{12}^{\text{Cu.v}}$; (c) Generalized vibration free energy levels: $X_0^{\text{Au.v}}, \cdots, X_i^{\text{Au.v}}, \cdots, X_{12}^{\text{Au.v}}$; (d) Generalized vibration free energy levels: $X_0^{\text{Cu.v}}, \cdots, X_i^{\text{Cu.v}}, \cdots, X_{12}^{\text{Cu.v}}$

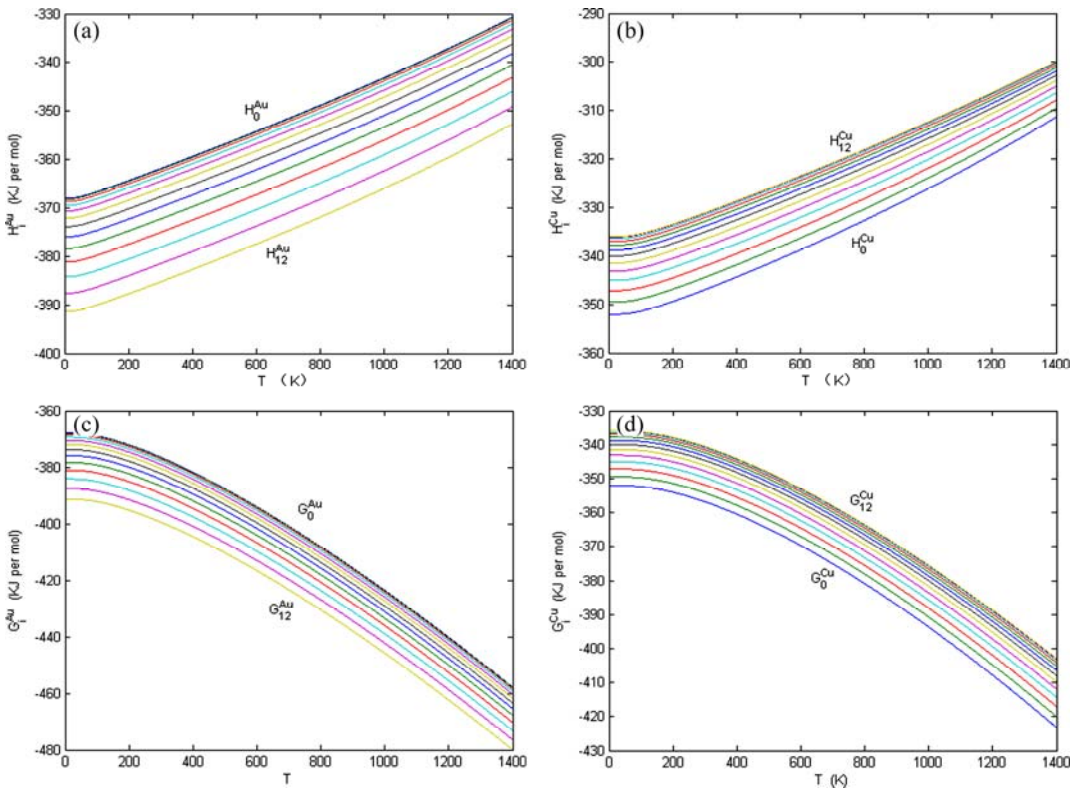


Fig. D.4 Curves of AG-thermodynamic properties in Au–Cu system: (a) Enthalpy of formation levels: $H_0^{\rm Au},\cdots,H_i^{\rm Au},\cdots,H_{12}^{\rm Au}$; (b) Enthalpy of formation levels: $H_0^{\rm Cu},\cdots,H_i^{\rm Cu},\cdots,H_{12}^{\rm Cu}$; (c) Gibbs energy levels: $G_0^{\rm Au},\cdots,G_i^{\rm Au},\cdots,G_{12}^{\rm Au}$; (d) Gibbs energy levels: $G_{12}^{\rm Cu},\cdots,G_i^{\rm Cu},\cdots,G_0^{\rm Cu}$

References

- SLATER J C. Electronic structure of alloys [J]. Journal of Applied Physics, 1937, 8(6): 385–396.
- [2] ELLIS D E, AVERRILL F W. Electronic structure of FeCl₄ anions in the Hartree-Fock-Slater model [J]. J Chem Phys, 1974, 60(8): 2856–2864.
- [3] BAERENDS E J, ELLIS D E, ROS P. Self-consistent molecular Hartree-Fock- Slater calculations. I. The computational procedure [J]. Chem Phys, 1973, 2(1): 41–51.
- [4] KIKUCHI R. A theory of cooperative phenomemena [J]. Phys Rev, 1951, 81(6): 988–1003.
- [5] KIKUCHI R, de FONTAINE D, MURAKAMI M, NAKAMURA T. Ternary phase diagram calculations—II. Examples of clustering and ordering systems [J]. Acta Metallurgica, 1997, 25(2): 207–219.
- [6] ASTA M, de FONTAINE D. First-principles study of phase stability of Ti-Al intermetallic compounds [J]. J Mater Res, 1993, 8(10): 2554-2568.
- [7] OATES W A, ZHANG F, CHEN S L, CHANG Y A. Improved cluster-site approximation for the entropy of mixing in multicomponent solid solutions [J]. Physical Review B, 1999, 59(17): 11221–11225.
- [8] OZOLINŠ V, WOLVERTON C, ZUNGER A. Cu-Au, Ag-Au, Cu-Ag, and Ni-Au Intermetallics: First-principles study of temperature-composition phase diagrams and structures [J]. Physical Review B, 1998, 57(12): 6427–6443.
- [9] BRAGG W L, WILLIAMS E J. The effect of thermal agitation on atomic arrangement in alloys [J]. Proceedings the Royal of Society A, 1934, 145(2): 699–730.
- [10] BRAGG W L, WILLIAMS E J. The effect of thermal agitation on atomic arrangement in alloys II [J]. Proceedings the Royal of Society A, 1935, 51(2): 540–566.
- [11] ORIANI R A. Thermodynamics of order alloy. II. The gold-copper system [J]. Acta Metall, 1954, 2(3): 608-615.
- [12] RHINES F N, BOND W E, RUMMEL R A. Constitution of order alloys of the system copper-gold [J]. Trans Amer Soc Met, 1955, 47(2): 578–597.
- [13] KAUFMAN L, BERNTEIN H. Computer calculation of phase diagrams [M]. New York: Academic Press, 1970: 225.
- [14] SUNDMAN B, FRIES S G, OATES W A. A thermodynamic assessment of the Au-Cu system [J]. Calphad, 1998, 22(3): 335-354.
- [15] SUNDMAN B, FRIES S G, OATES W A. A calphad assessment of the Au-Cu system using the cluster variatiation method [J]. Z Metallkd, 1999, 90(5): 267-273.
- [16] HILLERT M. The compound energy formalism [J]. Journal of Alloys and Compounds, 2001, 320(1): 161–176.
- [17] OATES W A. Configurational entropies of mixing in solid alloys [J]. Journal of Equilibria of Diffusion, 2007, 28(1): 79–89.
- [18] OSTP. Materials genome initiative for global competitiveness [R]. Washington DC: Office of Science and Technology Policy, 2011.
- [19] KAUFMAN L, ÅGREN J. First and second generation-birth of the materials genome [J]. Scripta Materialia, 2014, 70(1): 3–6.
- [20] SUTCLIFFE C H, JAUMOT F E Jr. Order-disorder in Au-Cu alloy. I. Short-range order in an alloy containing atomic percent Au [J]. Acta Metall, 1953, 1(2): 725–730.
- [21] JAUMOT F E Jr, SUTCLIFFE C H. Order-disorder in Au-Cu alloy.

- II. The nature of the order-disorder transformation and long-range order [J]. Acta Metall, 1954, 2(2): 63-74.
- [22] SCOTT R E. New complex phase in the copper-gold system [J]. Journal of Applied Physics, 1960, 31(12): 2112-2117.
- [23] LANG H, UZAWA H, MOHI T, PFEILER W. L1₂-long-range order in Cu₃Au: Kinetics and equilibrium as studied by residual resistivity [J]. Intermetallics, 2001, 9(1): 9–24.
- [24] KEATING D T, WARREN B E. Long-range order in beta-brass and Cu₃Au [J]. Journal of Applied Physics, 1954, 22(3): 286–290.
- [25] BUTLER B D, COHEN J B. The structure of Cu₃Au above the critical temperature [J]. J Applied Physics, 1989, 65(6): 2214–2219.
- [26] XIE You-qing. Systematic science of alloys [M]. Changsha: Central South University Press, China, 2012: 29–48.
- [27] XIE You-qing, LI Xiao-bo, LIU Xin-bi, NIE Yao-zhuang, PENG Hong-jian. Alloy gene Gibbs energy partition function and equilibrium holographic network phase diagrams of AuCu-type sublattice system [J]. International Journal of Communications, Network and System Sciences, 2013, 12(6): 415–442.
- [28] XIE You-qing, PENG Hong-jian, LIU Xin-bi, LI Xiao-bo, NIE Yao-zhuang. New atom movement mechanism for tracking path on disordering AuCuI(A₈^{Au} A₄^{Cu}) compound [J]. Transactions of Nonferrous Metals Society of China, 2014, 24(10): 3221–3256.
- [29] FEUTALAIS Y, LEGENDRE B, GUYMONT M. New enthalpies determination and in situ X-ray diffraction observations of order/disorder transitions in Au_{0.5}Cu_{0.5} [J]. Acta Materials, 1999, 47(8): 2539–2551.
- [30] XIE You-qing, ZHANG Xiao-dong. Electronic structure of Au-Cu alloys [J]. Science in China: Series E, 1998, 41(3): 225-236.
- [31] XIE You-qing, MA Liu-ying, ZHANG Xiao-dong, ZHOU Ping, ZHAO Li-ying. Microstructure and properties of Cu-Ni alloy [J]. Science in China: Series A, 1993, 36(5): 612–623.
- [32] ORIAN R A. Thermodynamics of ordering alloys. II. The gold-copper system [J]. Acta Metall, 1954, 2(7): 608–615.
- [33] JAUMOT F E, SUTCLIFFE C H. Order-disorder in Cu–Au alloys. II The nature of order-disorder transformation and long-range order [J]. Acta Metall, 1954, 2(7): 63–74.
- [34] XIE You-qing, LIU Xin-bi, PENG Hong-jian, LI Xiao-bo, NIE Yao-zhuang, LI Yan-fen. Characteristic atom arranging crystallography of alloy phases for Au-Cu system [J]. Science in China: Tech Sci, 2011, 54(6): 1560–1567.
- [35] DINSDALE A T. SGTE data for pure elements [J]. Calphad, 199l, 15(4): 317–425.
- [36] CAO W, CHANG Y A, ZHU J, CHEN S, OATES W A. Thermodynamic modeling of the Cu–Ag–Au system using the cluster/site approximation [J]. Intermetallics, 2007, 15(8): 1438–1446.
- [37] WEI S H, MBAYE A A, FERRIRA L G, ALEX Z G. First-principles calculations of the phase diagrams of noble metals: Cu–Au, Cu–Ag and Ag–Au [J]. Phys Rev B, 1987, 36(20): 4163–4185.
- [38] XIE You-qing. A new potential function with many-atom interaction in solid [J]. Science in China: Series A, 1993, 36(1): 90–99.
- [39] XIE You-qing. Electronic structure and properties of pure iron [J]. Acta Metallurgica et Materials, 1994, 42(11): 3705–3715.
- [40] XIE You-qing, ZHANG Xiao-dong. Electronic structure and properties of pure cobalt [J]. Science in China: Series E, 1996, 39(4): 394–403

AuCu₃-亚格子系统的合金基因 Gibbs 能配分 函数和平衡全息网络相图

谢佑卿 1,2,3, 李小波 4, 刘心笔 1,2,3, 聂耀庄 5, 彭红建 6

- 1. 中南大学 材料科学与工程学院,长沙 410083;
- 2. 中南大学 粉末冶金研究院, 长沙 410083;
- 3. 中南大学 粉末冶金国家重点实验室, 长沙 410083;
 - 4. 湘潭大学 材料科学与工程学院,湘潭 411105;
 - 5. 中南大学 物理与电子学院,长沙 410083;
 - 6. 中南大学 化学化工学院,长沙 410083

摘 要:以 AuCu₃-亚格子系统为例,介绍 3 项发现:第一,迄今阻碍金属材料科学进步的第三大障碍是研究者们习惯用平衡均匀转变的思维方式认识温度极其缓慢变化的合金相变实验现象,然后以实验现象的错误认识为选择信息,建立 Gibbs 能函数和所谓的"平衡相图";第二,AuCu₃-型亚格子系统的平衡全息网络相图可用来描述与成分和温度有关的合金基因排列结构和各种热力学性质的系统相关性;第三,每个合金的平衡转变都是均匀的单相转变,不是非均匀的双相转变,存在一条没有有序相和无序相共存区的单相相界线,相界线顶点成分和温度远偏离 AuCu₃ 化合物临界点的计量成分和温度。

关键词: $AuCu_3$ 化合物; $AuCu_3$ -型亚格子系统; 合金基因 Gibbs 能配分函数; 平衡全息网络相图; 系统金属材料 科学

(Edited by Yun-bin HE)